Article:

Marini, M, Felletti, F, Milli, S et al. (1 more author) (2016) The thick-bedded tail of turbidite thickness distribution as a proxy for flow confinement: examples from Tertiary basins of central and northern Apennines (Italy). Sedimentary Geology, 341. pp. 96-118. ISSN 0037-0738

https://doi.org/10.1016/j.sedgeo.2016.05.006

The thick-bedded tail of turbidite thickness distribution as a proxy for flow confinement: examples from Tertiary basins of central and northern Apennines (Italy)

Mattia Marini[1], Fabrizio Felletti[1], Salvatore Milli[2] and Marco Patacci[3]

[1]Earth Science Department 'Ardito Desio', University of Milan, Italy.
[2]Earth Science Department, University of Rome 'Sapienza', Italy
[3]Turbidites Research Group, School of Earth and Environment, University of Leeds, Leeds, LS2 9JT, UK
Contact details: mattia.marini@unimi.it; ++393405865715

Abstract

The assessment and meaning of turbidite thickness statistics represent open research questions for both applied and pure sedimentology. Yet thickness data collected in the field are often incomplete and/or biased toward or against certain thickness classes due to bed geometry, erosion and/or operational filed constraints, which largely undermine tackling such questions. However, in situations where turbidity currents are ponded by basin topography so to deposit basin-wide tabular beds and erosion is negligible, some of the variables of the 'bed thickness equation' can be relaxed, making easier to investigate what the primary controls on turbidite thickness statistics are. This study reviews the bed thickness statistics of the non-channelized parts of the infill of four tertiary basins of Central-Northern Apennines (Italy), where bed geometry and sedimentary character have been previously assessed. Though very different in terms of size and, arguably, character of feeder system and source area, these basins share a common evolution to their turbidite fill with upward transition from an early ponded to a late unconfined setting of deposition. Based on comparison of thickness subsets from diverse locations and stratigraphic heights within the basin fills of the case studies, this paper seeks to answering the following questions: i) how data collection choices and field operational constraints (e.g. location, outcrop quality, use of thickness from single vs. multiple correlative sections, length of the stratigraphic section from which thicknesses were retrieved) can affect statistics of an empirical distribution of turbidite thicknesses? ii) how depositional controls of confined vs. unconfined basins can modify the initial thicknesses distribution of turbidites?; iii) is there in turbidite thickness statistics a 'flow confinement' signature which can be used to distinguish between confined and unconfined depositional settings? Results suggests that: i) best practices of data collection are crucial to a meaningful interpretation of turbidite thickness data, especially in presence of stratigraphic and spatial trends of bed thickness; ii) a systematic bias against cm-thick Tcd *Bouma* sequence turbidites deposited by small volume low density flows exists, which can significantly modify the low-end tail of an empirical frequency distribution of bed thickness; iii) thickness statistics of beds starting with a basal Ta/Tb *Bouma* division bear a coherent relationship to the transition from ponded to unconfined depositional settings, consisting in a reduction of variance and mean and, consequently, modification of the initial thickness-frequency scaling relationship. This research highlights the role of flow stripping, sediment by-pass and bed geometry in altering the initial thickness distribution of ponded turbidites suggesting how, on the contrary, fully ponded mini-basins represents the ideal setting for further research linking turbidite thickness statistics and frequency distribution of parent flow volumes.

Keywords: *turbidites, bed thickness statistics, turbidite bed geometry, confined basin, flow ponding, flow stripping*

1. Introduction

Thickness variability of beds deposited by turbidity currents (turbidites hereafter) represents a meaningful yet complex record of flow characteristics, flow-bathymetry interaction and bed shape. Turbidite thickness data retrieved from a borehole are important in hydrocarbon system modelling (Flint and Bryant, 1993) for estimation of reservoir rock volumes. Significant research efforts has been dedicated to understand whether the frequency distribution of turbidite thicknesses should follow a generic law, but they ended up documenting a great diversity of empirical distributions (see Pickering and Hiscott, 2015 for an overview). This diversity primarily reflects a combination of first order controls such as statistical distribution of inbound flow volumes, flow rheology, basin-floor topography, turbidite bed shape, etc. (Hiscott et al., 1992, 1993; Rothman et al., 1994; Rothman and Grotzinger, 1996; Awadallah et al., 2001; Carlson and Grotzinger 2001; Talling, 2001; Chakraborty et al., 2002; Sinclair and Cowie, 2003; Felletti and Bersezio, 2010; Pantopoulos et al., 2013). However, it is widely acknowledged that measured distributions might constitute incomplete or biased representations of the actual thickness population owing to a number of factors, (e.g. outcrop/core quality, measure/borehole location and thickness of studied/cored interval; see for example Drummond and Wilkinson, 1996; Malinverno, 1997). Notwithstanding the incompleteness of measured distributions, the challenge in interpreting turbidite thickness statistics resides in the fact that some of the variables (e.g. bed volume and shape, including lateral extent and pinch-out geometry) are unknown *a priori* and likely to be interdependent via complex feedbacks (Janoko, 2010). In situations where erosion is negligible and turbidites are basin-wide and tabular, some of the variables (e.g. bed shape, measure location, sampling biases) of the turbidite thickness statistics paradigm can be fixed, making easier to study other controls (input volumes, depositional controls intrinsic to confinement etc). This condition is commonly met in small turbidite basins enclosed by a confining topography (i.e., confined basins; see Lomas and Joseph, 2004), where flows large enough can spread over the entire depocentre and become ponded, therefore depositing basin-wide sheet-like turbidites (see paragraph 2.1).

This study investigates the stratigraphic variability of bed thickness statistics of the distal non-channelized parts of four confined to unconfined turbidite units of northern and central Italy, the 'Cengio, Bric la Croce – Castelnuovo' turbidite systems and Castagnola Formation of the Tertiary Piedmont Basin and the Laga and Cellino formations of the Apennines foreland basin system.

The primary focus of this paper is nor finding a general statistical model for turbidite thickness distribution, neither methods for best-fitting empirical data, on which the literature is vast (Goldstein et al., 2004; Clauset et al. 2009; Sylvester, 2007; Cirillo, 2013). Instead, this paper aims at answering the following questions: i) how do data collection choices and/or field operational constraints (e.g. use of thickness from single vs. multiple correlative sections, length of the stratigraphic section, location with respect to basin topography, outcrop quality etc.) affect the statistical appraisal of frequency distribution of turbidite thicknesses? ii) Is there a turbidite thickness statistics signature of flow confinement that can be used to distinguish between confined and unconfined depositional settings? iii) How do depositional controls of confined vs. unconfined basins modify the initial thicknesses distribution of turbidites?

2. Overview of turbidite thickness statistics

Early research on frequency distribution of turbidite thickness mostly focused on finding which model better described empirical datasets, and if such a law was somehow generic to turbidite deposition (e.g. truncated Gaussian, lognormal, exponential and power-law; see Sylvester, 2007 for an overview). In most of these studies, distribution models better describing empirical thickness populations were chosen through visual inspection of a number of graphical tools, such as histograms and log-log plots of exceedance probability (i.e. plots with logarithmic scale on both horizontal and vertical axes relating the number of beds thicker than a given thickness *h,* to *h;* Fig. 1). However, as case studies grew in number, it became obvious that, other than sharing an inverse relationship of thickness against number of beds (i.e. thinner beds are more numerous that thicker beds), empirical distributions departed significantly from simple statistical models and differed greatly from each other, especially in their thin-bedded tails (see Pickering and Hiscott, 2015 for an overview). Based on the assumption that a generic law describing turbidite thickness existed, a number of factors (e.g., sampling bias against thin beds, non-deposition by small volume flows not reaching the sampling site, erosion; Drummond and Wilkinson, 1996) were used to explain scarcity of very thin beds in log-normal distributions (McBride, 1962; Ricci Lucchi, 1969; Ricci Lucchi and Valmori, 1980; Murray et al., 1996) and in truncated Gaussian distributions (Kolmogorov, 1951; McBride, 1962; Mizutani and Hattori, 1972) when compared to exponential distributions (Muto, 1995; Drummond, 1999; see also Chakraborty et al., 2002). For analogy with some of the most common triggers of turbidity currents (e.g., submarine sand avalanche and earthquakes) and other geological quantities (e.g., fault lengths, volcanic eruptions and drainage networks; Turcotte, 1997), another line of thought (Hiscott et al., 1992, 1993; Beattie and Dade, 1996; Rothman et al., 1994; Rothman and Grotzinger, 1996) proposed that the frequency distribution of turbidite thickness should follow a power-law exceedance probability equation:

$$N(H>h) = N_{total}h^{-\beta} \quad (1)$$

where N is the number of beds of thickness H greater than h, N_{total} is the total number of beds and β is the scaling exponent of the power-law relationship. Equation (1) plots as a straight line on a bi-logarithmic (log-log) graph (Fig. 1) and is typically valid above a threshold value or lower bound denoted as x_{min}. An implication of such power-law relationship is that the bed thickness distribution is scale invariant and completely described by the scaling exponent β, which would therefore represent a fractal dimension (Turcotte, 1997). Due to the great popularity of fractality in nature, from the 1990s onwards most of the empirical distributions showing convex-upward shapes on a log-log exceedance probability plot were interpreted as 'segmented' distributions resulting from modification of a power-law input signal (i.e. the distribution of volumes of flows entering the basin). The sharp cross-over in the scaling exponent β of 'segmented' distributions was variously interpreted as resulting from sampling biases, erosion and/or undetected amalgamation, flow rheology transitions and flow-basin topography interactions (Rothman and Grotzinger, 1995; Malinverno, 1997; Chen and Hiscott, 1999; Carlson and Grotzinger, 2001; Awadallah et al., 2002; Sinclair and Cowie, 2003; Felletti and Bersezio, 2010). The power-law paradigm was later challenged on the ground that 'segmented' distributions can result from mixing of two or more sub-populations of beds each characterized by a log-normal distribution (Talling, 2001; Sylvester, 2007; Pantopoulos et al., 2013). In this 'log-normal mixture' model, the sub-populations are characterised by different basal grain size or sedimentary structures and the sharp gradient cross-over of many thickness probability plots is interpreted as associated to differences in the parent flow (e.g. low density vs. high density turbidity currents).

2.1. Controls on deposition of ponded turbidites and on resulting bed thickness statistics

In turbidity currents' mechanics, confinement is the ability of the seafloor topography to obstruct or redirect the flow thereby inducing perturbation of its velocity field and physical structure (Joseph and Lomas, 2004). Interaction with obstacles of size comparable to or larger than the height of incoming flows, such as bounding slopes of enclosed mini-basins, can result in a range of modifications within the flow (e.g. reflection/deflection, constriction, ponding and flow stripping; see Patacci et al., 2015), producing unusual vertical sequences of sedimentary structures (Kneller et al., 1991; Haughton, 1994; Kneller and McCaffrey, 1999; Bersezio et al., 2005, 2009; Tinterri 2011). Upon impact onto bounding slopes, the density stratification of turbidity currents typically results in trapping of the lower, higher-density and sandier part of the flow in the deeper part of the basin and stripping (*sensu* Sinclair and Tomasso, 2002) of the more dilute and muddier upper part of the flow, which can partially escape the basin by surmounting the topography or overflowing a local sill. Ponding represents a case of confinement, whereby the entire flow is trapped by the topography (Van Andel and Komar, 1969). When sustained large flows are discharged into a receiving basin, flow ponding can result in the development of a flat-topped sediment cloud (i.e. the ponded suspension cloud; Toniolo et al., 2006; Patacci et al., 2015). Ponding and flow stripping processes are intimately related in that if the total volume discharged by a turbidity current is larger than the volume of the receiving basin, the ponded suspension cloud can thicken up to partially overflow the confining topography (Patacci et al., 2015; Marini et al., 2016), with establishment of partially ponded conditions. The most striking sedimentary signature of ponding are basin-wide couplets of sands with multiple repetitions of sedimentary structures and relatively thick co-genetic mud caps (Ricci Lucchi and Valmori, 1980; Pickering and Hiscott, 1985; Haughton, 1994; Kneller and McCaffrey, 1999). Conversely, similarly to by-pass in unconfined systems, in partially ponded conditions, flow stripping can deplete turbidites of their finer-grained fraction resulting in sandstones with unusually thin fine-grained laminated tops and mud caps (Sinclair and Tomasso, 2002; Marini et al., 2016). Common examples of confined-ponded turbidite systems are found in structurally-controlled elongated basins, such as wedge-top basins of foreland basin systems (Remacha et al. 2005; Milli et al., 2007, 2009; Tinterri and Tagliaferri, 2015), rift basins (Ravnås and Steel, 1997; Ravnås et al, 2000) and intraslope salt-withdrawal mini-basins (Prather et al. 2012). The initial topography of these basins is generally able to fully pond incoming flows (i.e. all the sediment is trapped within the basin) leading to development of a sheet-like architecture. However, when sedimentation rate outpaces tectonic deformation, sediment infilling can result in enlargement of the local depocentre and decrease of the height of the enclosing slopes. Consequently, the degree of flow confinement decreases and the proportion of sediments escaping the basin increases (Remacha et al. 2005; Felletti and Bersezio, 2010; Marini et al. 2015, 2016), in a manner similar to that described by the classical ‘fill to spill’ model of Sinclair and Tomasso (2002).

The effect of confinement on turbidite thickness distribution is amenable to numerical experiments (Malinverno, 1997; Sylvester, 2007), simulating measurement of bed thickness along a vertical sampling line located at the centre of a circular enclosed mini-basin. These experiments used a large number of model beds turbidites with cylindrical shape, power-law volume frequency distribution and fixed scaling of bed length to thickness to demonstrate that if beds are placed at random within the basin then the log-log plot of exceedance probability of thicknesses measured along a sampling line at the basin centre will break into three linear segments (Fig. 2a). These segments correspond to subpopulations of: i) relatively thin turbidites with diameter smaller than the radius of the receiving basin, which form a first segment with slope β_{small} as a result of being undersampled (not all of them are encountered by the sampling line; ii) turbidites of intermediate thickness and diameter equal to or greater than the basin diameter, which are always intersected by the sampling line and form a segment of the distribution with slope β_{large} and iii) basin-wide turbidites (i.e. turbidites with diameter greater than the basin diameter), namely mega-beds that are ponded by the receiving topography, which form a linear segment of the distribution with slope $\beta_{large}>\beta_{mega}\geq\beta_{small}$ (Fig. 2a). As claimed by Sylvester (2007), though very simplistic with regard to geometry of model beds, the model of Malinverno (1997) might be able to produce ‘segmented’ power-law distributions with the provisos that volumes of incoming turbidity currents must show a power-law frequency distribution and bed thickness is measured at or very close to basin centre.

Other numerical experiments (Sinclair and Cowie, 2003) showed that if all the turbidity currents entering a mini-basin are ponded (i.e. all the sediment is trapped in the basin) and volumes of incoming flows follow a power-law distribution, then the resulting bed thicknesses will scale to volumes as a function of bed length and size of the mini-basin (Fig. 2b). Modifications of a power-law input signal have been also linked to flow stripping and erosional bed amalgamation (Sinclair and Cowie, 2003). Specifically, in partially ponded basins flow stripping of the upper and finer-grained part of large volume (and thicker) currents acts by limiting the total amount of sediment trapped in the basin so that the bed thickness population is depleted in its thick-bedded tail (Fig. 2b).

3. Methodology

The thickness data considered in this study were taken and revised from earlier works by the authors (Felletti et al., 2009; Felletti and Bersezio, 2010; Marini et al. 2015, 2016), to which the reader is referred for details of the locations and sedimentological descriptions. The compound database therefore comprises as many datasets as the studied turbidite units (Table 1), each consisting of a number of stratigraphic and location subsets, i.e. sets of thickness measures collected from specific stratigraphic intervals of the case study on a single section within the basin. As discrimination of hemipelagic from turbiditic mudstone was not always practical due to outcrop quality, thereby preventing in some instances to correctly place the upper boundary of turbidite event beds and measure their thickness, the choice was made to work with sandstones only. Therefore, if not specified otherwise, 'bed thickness' is used here to refer to the sandstone part of turbidites. Bed thickness was measured from the base of the sandstone to the boundary between very fine silty sandstone and mudstone, using a tape meter for thinner beds (thickness range 1-50 cm) and a Jacob's staff for beds thicker than c. 50 cm (see Patacci, 2016 for a review on error sources when measuring bed thicknesses). The thickness of the mudstone above was recorded separately, noting whether the quality of the outcrop allowed it to be interpreted as a mud cap genetically related to the underlying turbidite sandstone. The basal grain size of the sandstone was measured using a magnifying lens and a grain size comparator, thereby allowing for detection of subtle grading breaks and correct placing of boundaries of single event beds within amalgamated bedsets. As it was believed that hybrid beds (*sensu* Haughton et al. 2009), namely beds deposited by flows including a frontal turbidity current and a lagging co-genetic debris flow, may have a significantly different depositional mechanism, after calculating their relative frequency (generally below 6%) they were excluded from the analysis. To facilitate comparisons across case studies, turbidites were classified according to the same bed type scheme, based on sedimentological character and grain size of their basal division. Two main bed type classes were distinguished: a) beds consisting of T_c and/or T_d Bouma (1962) divisions with typical basal grain size finer than 250 µm and thickness generally less than 30-50 cm, and b) beds starting either with a basal T_a or T_b *Bouma* divisions coarser than 250 µm which may grade upward into finer sands with variously developed $T_{c\text{-}d}$ divisions (thickness generally greater than 10-30 cm). Although there is much more complexity in the turbidites of the studied examples (for which the reader is referred to relevant literature given in Table 1), this simple bed type scheme has the advantage of objectively discriminating between two classes, namely the deposits of low and high density flows (see Lowe, 1982 and discussion in Talling, 2001). Prior to undertaking data analysis, an assessment of the effects of sampling procedures on thickness statistics was carried out by comparing subsets from different stratigraphic intervals and locations (see paragraph 5.1). Following such an assessment, further statistical analysis was focused only on thickness subsets from single sections either located as close as possible to the basin centre or, when basin shape was uncertain, the farthest possible from basinal slopes. Best fitting with three model distributions (i.e. exponential, log-normal and power-law) commonly used in turbidite thickness statistics was performed using the Easyfit software package. Easyfit uses the maximum likelihood estimation method (MLE) to assess parameters of log-normal and power-law fits whereas fitting with the exponential model is based on the method of moments. In both fitting methods, the number of iterations and the accuracy of MLE was set to 100 and 10^{-5}, respectively. Goodness-of-fit testing was accomplished with the same software using the Kolmogorov-Smirnov (K-S), the Chi-Squared ($\dot{X}^2$) and the Anderson-Darling (A-D) tests. All of these tests assess the compatibility of a random sample (i.e. the empirical distribution of turbidite thickness measured in the field) with a theoretical probability distribution function (i.e. the model distribution), that is how well the model distribution fits empirical data. This is accomplished computing test statistics (see for example Table 2) that quantify how much the cumulative distribution function of an empirical dataset departs from that of the model distribution and comparing the obtained values to standard tables of critical values compiled in the Easyfit for different significance levels (0.01, 0.05 etc.). In this study a significance level of 0.1 was applied, that is, there is 10% probability that the model distribution passing the tests is not an adequate fit. For $\dot{X}^2$ a equal probability binning was adopted which follows the law:

$$k = 1+log_2(N) \qquad (2)$$

where *k* is the number of bins and *N* the number of beds in the sample data. In addition to test statistics *p-values* are also computed in K-S and $\dot{X}^2$ which may be considered as a measure of plausibility of the model distribution being a good fit for the empirical distribution being tested. Specifically, while small values of *p* shed doubt on the goodness of the fit, large values of *p* do neither prove it nor demonstrate evidence against it. The most likely parent distribution reported in Table 2 were chosen taking into account goodness of fit results of the three tests and *p-values* jointly, with the provisos that since standard table for critical values were used, though equally with respect to whichever model, results of the tests are conservative.As the bed types subset for which a power-law model cannot be excluded based on the adopted goodness-of-fit tests comprised less then ≈50 beds, in agreement with the assessment of Clauset et al. (2009) on the minimum sample size (≈100) required for successfully distinguishing between a power-law and a log-normal as the best fit option, the decision was made to not implement the procedure for using of K-S proposed by these Authors. Yet, not using boothstrapping (see Clauset et al., 2009) for estimating the lower bound x_{min} of the power-law fit of bed types subsets, might not represent a limitation to the purpose of this study, as best fitting was intended for being tied to facies and parent flow characteristics rather than bed thickness alone.

As an independent mean to characterize the thick-bedded tails of our empirical frequency distributions and quantify their location and spread (i.e. statistical dispersion of a dataset), summary statistics including mean, quantiles, interquartile ranges (i.e. the difference between the

75% and the 25% quantiles) and coefficient of variation (i.e. the ratio of standard deviation to mean) were also calculated (Isaaks and Srivastava, 1989).

4. Case studies

The turbidite units considered in this study represent parts of the infill of the Tertiary Piedmont Basin of NW Italy and of the latest Miocene – early Pliocene Apennine foreland basin system of central Italy (Fig. 3 and Table 1). The Tertiary Piedmont Basin (TPB hereafter) is a relatively small yet complex wedge-top basin (Figs 3 and 4) located at the junction between the westward-verging stack of tectonic nappes of Western Alps and the north-eastward verging Northern Apennines (Mosca et al. 2010; Carminati and Doglioni, 2012; Maino et al. 2013; Ghibaudo et al., 2014a, b). It consists of two main sub-basins, namely the Langhe Basin to the west and the Borbera-Curone Basin to the east (Gelati and Gnaccolini, 1998; Mosca et al., 2010), which side the Alto Monferrato structural high (Fig. 4) and host up to 4000 m of continental to deep marine clastic sediments. The clastic infill of these sub-basin records Early Oligocene – Burdigalian extensional tectonics related to the opening of the Ligure-Provençal Basin (Gelati and Gnaccolini, 2003).

The foreland basin system of the Central Apennines is a large palaeogeographic domain developing from the Oligocene onwards in response to the westward subduction of a promontory of the African Plate (i.e. the Adria microplate) underneath the European plate (Malinverno and Ryan, 1986; Vai, 2001; Boccaletti et al., 1990; Carminati and Doglioni, 2012). Roll back of the subducting plate led to eastward migration of both the accrectionary wedge and the adjacent foredeep which was filled by diachronous turbidite units (Fig. 3) younging from west to east (Ricci Lucchi, 1986). These include four main foredeep turbidite infills, namely the Macingo Formation (Chattian-Burdigalian), the Cervarola-Falterona Formation (Burdigalian-Langhian), the Marnoso Arenacea Formation (Langhian-Lower Messinian) and the Cellino Formation (Lower Pliocene; see paragraph 4.4) supplied axially with sediments from Alpine sources. A number of smaller turbidite bodies of Messinian age (including the Laga Formation, see paragraph 4.3) were also deposited within scattered structurally-confined wedge-top basins (‘bacini minori’ of Centamore et al, 1978) with mostly transverse feed (Fig. 3). Establishment and infilling of these basins records the accretion of the Marnoso Arenacea into the orogenic wedge (Ricci Lucchi, 1986; Manzi et al., 2005) and pre-dates the onset of the late Messinian – Pliocene periadriatic foredeep, respectively.

The Castagnola Formation (**CS**). It represents the infill of one of the sub-basins of the Borbera-Curone sector (Castagnola Basin; Fig. 4) and consists of a >950 m-thick turbidite succession of Late Chattian-Early Burdigalian age. It was deposited in a slightly elongated structural depression forming southward of the ENE–WSW striking Villalvernia-Varzi Line (V-V in Fig. 4; Cavanna et al., 1989; Mutti, 1992; Stocchi et al., 1992, Di Giulio and Galbiati, 1998) and running parallel to it. **CS** has been subdivided into three members (Baruffini et al., 1994), namely, from older to younger, the Costa Grande, Arenaceo and the Brugi Marls members. While the older two members are represented almost exclusively by turbidites, the younger Mt. Brugi Marls Member consists of mostly silicified marly hemipelagites with intercalations of thin bedded turbidites. Well exposed onlaps onto basinal slopes (Felletti, 2002; Southern et al., 2015) indicate an initial depocentre with size of c. 4x2 km (length x width) which might have increased up to a minimum of c. 6x4 km (length x width) as a result of infilling by turbidites of the Costa Grande Member. Early research (Cavanna et al., 1989; Stocchi et al., 1992) documented a change in architectural style from the sheet-like and relatively mud-rich Costa Grande Member, consisting of basin-wide sandstone-mudstone couplets, to the sand-rich Arenaceo Member. typified by lenticular and locally amalgamated turbidite sandstones. More recently, stratigraphic trends in sand-to-mud ratio and facies have been interpreted to reflect the transition from a dominantly ponded sheet-like system (Costa Grande Member) to a non-ponded system (Arenaceo Memmber) (Marini et al., 2016).

The stratigraphy and process sedimentology of the **CS** has been recently addressed (Marini et al., 2016) by means of a highly detailed sedimentological section logged at the basin centre. The most significant stratigraphic trend in this turbidite unit is the steady increase in sand-to-mud ratio from base to top. In the uppermost c. 200 m of the studied section this is accompanied with replacement of basin-wide sandstone-mudstone cap couplets with a ponded character (bed types A and B of

Southern et al., 2015 *cf*. 'contained beds' of Pickering and Hiscott, 1985; see also Haughton, 1994; Sinclair, 1994), by locally amalgamated turbidites with thin fine-grained tops (bed type B' of Marini et al., 2016) suggestive of by-pass. In addition, whilst *Bouma*-like T_{cd} turbidites (bed types D of Southern et al., 2015; typically thinner than c. 30 cm) are ubiquitous in the studied section forming a background to clusters of thicker beds, their relative frequency appear to decrease upward in the stratigraphy. These trends culminate in the transition from a lower, relatively shale-prone sections (unit 1 and unit 2 of Marini et al. 2016; **CS-1** and **CS-2** hereafter) punctuated by thick beds with a ponded character, including thick mud caps, by a upper sand-rich section where by-pass of fines and event bed amalgamation dominate (unit 3; **CS-3** hereafter). If thicknesses of mud caps of turbidites from **CS-1** and **CS-2** are looked at into greater detail, a weak but negative correlation of their thickness proportion and total thickness of event beds to which they belong can be seen, hinting at some dependency of the amount of mud the basin topography was able to trap on total volume of incoming turbidity currents. The stratigraphy of **CS** was interpreted as embodying a threefold 'fill to spill' evolution of the host basin (Marini et al., 2016), including: i) an early ponded stage (**CS-1**) in which only part of the mud of exceptionally large flows could escape the basin, ii) an intermediate stage (**CS-2**) when levelling of the initial topography by turbidite infilling resulted in enhanced flow spilling, possibly affecting also a fraction of the sand of exceptionally large flows and iii) a late by-pass stage (**CS-3**) where turbidite systems were virtually unconfined and could expand over an healed topography.

Cengio (CTS) and Bric la Croce - Castelnuovo (BCTS) turbidite systems. These are two superimposed turbidite systems of Late Oligocene age infilling a structurally-confined depocentre set along the western slope of the Langhe Basin of TPB (Fig. 4) (Gelati and Gnaccolini, 1980; Cazzola et al., 1981, 1985; Mutti, 1992; Gelati and Gnaccolini, 1998, 2003; Felletti and Bresezio, 2010; Felletti, 2016). Deposition of **CTS** and **BCTS** took place in a period of quiescent tectonics (sequences B2-3 of Gelati and Gnaccolini, 1998) within a SW-NE-trending structural trough supplied with turbidity flows from the southwest. While the southern, western and northern bounding slope of the **CTS** - **BCTS** depocentre are well exposed, uncertainty exists about the eastern margin of the basin, which might have been located a few km away from the studied outcrop, i.e. at the structural culmination of basement rocks (Gelati and Gnaccolini, 1980; Cazzola et al., 1981). The transition from ponded sheet-like turbidites of the lower **CTS** (sandbodies I and II; Bersezio et al. 2005, 2009) to unconfined lobes of the **BCTS** via non-ponded, but laterally confined lobes of the upper **CTS** (sandbodies III-VIII; Bersezio et al., 2009) is interpreted to reflect a significant enlargement of the local depocentre due to sediment infill (Felletti and Bersezio, 2010; Felletti, 2016).

Based on numerous stratigraphic sections from different locations with respect to basinal slopes, previous workers (Bersezio et al., 2005, 2009; Felletti and Bersezio, 2010) documented an increased degree of bed amalgamation and sand-to-mud ratio toward onlap terminations and greater proportions of massive sands at the base of confining slopes. Coupled with palaeoflow indicators, these trends suggest redirection and blocking of the lower, denser part of flow. Conversely, from proximal to distal (i.e. from SW to NE), Bersezio et al. (2005) reported a decrease in sand-to-mud and laminated-to-massive sandstone ratios and average thickness of the sandstone beds.

Away from basinal slopes, the most common bed type in both **CTS** and **BCTS** is represented by massive to laminated, graded sandstones with very thin or missing rippled tops (top-missing *Bouma* sequences; *cf* bed types D, E and DB of Bersezio et al. 2005). These beds occur in both thin bedded, well stratified mud-prone intervals and sand-rich packages. In the latter, they can lack any mud cap and be welded to form amalgamated bedsets, but only rarely show basal scours (up to a few cm's deep), suggesting little erosion from subsequent flows. Other bed types include variously developed *Bouma*-like sequences, which can be either complete or miss Ta/Tb divisions. In **CTS** these beds can internally show repeated sequences of sedimentary structures ('complex' beds *sensu* Bersezio et al. 2005, 2009), interpreted as the product of instabilities induced in the flow by interaction with basinal slopes (see Kneller and McCaffrey 1999; Tinterri, 2011). Whichever the bed type, it is noteworthy that the thickness of the sandstone and the mud cap of event beds have only very limited negative correlation, with thicker beds showing thinner mud caps with respect to thinner beds. The widespread by-pass indicators (e.g. reduced thickness of fine-grained rippled tops and mud caps, hints of anticorrelation of mud cap and sandstone thickness within event beds) in both **CTS** and **BCTS,** coupled with proximal to distal variability in bed thickness and mud content (Bersezio et al., 2005) indicates that, while incoming turbidity currents unquestionably interacted with the north and north-western basinal slopes, neither their sandy nor muddy part were ponded by the receiving topography over most of the studied section.

The Laga Formation lobes (**LG**). The Laga Formation constitutes the c. 3000-thick turbidite infill of a relatively large wedge-top basin (i.e. the Laga Basin; Figs 3 and 5b) developed since the late Tortonian in response to tectonic fragmentation of the Marnoso Arenacea foredeep (Manzi et al., 2005; Milli et al., 2007). **LG** is composed of five unconformity-bounded units (Laga 1a, 1b, 1c, 2 and 3), correlatable to main tectonic-stratigraphic events of the Messinian (Milli et al., 2007, 2009, 2013). They can be grouped into two high rank depositional sequences, namely the Laga Depositional Sequence (Laga 1a-c and Laga 2, upper Tortonian-lower Upper Messinian) and the Cellino Depositional Sequence (Laga 3 and younger deposits of the Vomano and Cellino Fms.; Upper Messinian – Lower Pliocene). These sequences display a eastward stacking and are separated by a main erosional unconformity (the intra-Messinian unconformity) recording an acme of tectonic shortening and uplift along the thrust front of Central Apennine (Ricci Lucchi, 1986; Manzi et al., 2005; Milli et al., 2007). The deposition of the Laga 1a-c and Laga 2 took place in a confined 'piggy-back' basin swallowing and enlarging as a result of turbidite infill (Fig. 5a), whereas the Laga 3 unit records the onset of the Pliocene to present-day foreland basin systems (Milli et al., 2007, 2009; Bigi et al. 2009). From north to south, physical stratigraphy and facies analysis of the Laga 1-2 turbidite systems document along-stream transition from proximal distributive networks of low-sinuosity channels to distal lobes (i.e., **LG**) and an overall stratigraphic evolution from a more confined to less confined setting of deposition (Milli et al., 2007, 2009, 2013; Marini et al., 2015).

The thickness data used in this study come from three superimposed lobe units, namely, from older to younger, the Poggio Umbricchio (**LG-1**), the Crognaleto (**LG-2**) and the Mt. Bilanciere (**LG-3**) lobe complexes, deposited in a depocentre enlarging considerably (by a factor in excess of 3.5, see Table 1) as a result of infilling from turbidites. **LG-1** has the highest sand-to-mud ratio compared to the two younger lobe complexes and it is characterized by higher proportion of massive-looking dewatered sandstones, coarser and less sorted grain size and thinner mud caps. It has been suggested that while the structureless character of the sandstones of LG-1 might reflect rapid sediment dumping resulting from blocking of the flows by the confining topography, the low mud content in the same unit would indicate either spilling of finer grained sediments or an initial coarser-grained sediment input (Marini et al. 2015). Two contrasting styles of depositional architecture have been recently documented in these units, specifically a sheet-like architecture composed of mostly basin-wide event beds, such as that of the two older complexes (**LG-1** and **LG-2**), and a ‘jig-saw-like’ architecture typified by the laterally shifting lobes of the younger complex (**LG-3**) (Marini et al. 2015). Lateral facies changes in beds of **LG-1** and **LG-2** are limited to the vicinity of bounding slopes thus reflecting a primary control from flow-topography interactions. On the contrary, beds of **LG-3** show a higher but regular lateral variability in bed character (thickness, grain size and proportion of massive vs. laminated sands decrease from proximal to distal and across palaeoflow) suggestive of deposition from unconfined turbidity currents losing competence and capacity away from the centre of mass of lobes. In all the units, thin bedded *Bouma*-like T_{cd} turbidites cluster into metre to decametre-scale packages correlatable over most of the depocentre without significant changes in facies, grain size and sand content, suggesting they are unlikely to represent turbidite lobe fringes.

As suggested by the increase in size of the local depocentre, the change of architectural style was interpreted as a shift from partially ponded (**LG-1**) and confined (**LG-2**) conditions, to unconfined conditions (**LG-3**) favouring deposition of lobate sandbodies with compensational stacking (Marini et al. 2015; see also Mutti and Sonnino, 1981).

Cellino Formation (CL). This turbidite unit of Early Pliocene age represents the over 2500m-thick infill of the inner sector (namely, the Cellino Basin) of the Pliocene to present-day foreland basin system of the Apennines. Due to limited outcrop, most of the knowledge about the size and geometry of the Cellino Basin is owed to a wealth of seismic and well data made available by the intense hydrocarbon exploration undertaken from the 50's to the 70's of the last century (Casnedi et al., 1976 Casnedi, 1983; Vezzani et al. 1993) (Figs. 3 and 5). Correlation between outcrops and geophysical well logs allowed tracking **CL** in the subsurface for over c. 40 km and up to 150 km in a E-W and N-S directions, respectively (Carruba et al. 2004, 2006), and detailing the architecture of its six members (A to F from top to bottom; Casnedi, 1983).

This study focuses on the c. 750 m-thick sand-rich section of the E member only, which represents the early confined infill of a N-S trending foredeep supplied with flows from the north (Felletti et al. 2009). The thickness data presented in this paper are located in the southernmost part of the basin (Barricello section; see Felletti et al. 2009 for details). Lateral thickness changes in the older F member reveal some initial unevenness of the seafloor at the onset of turbidite deposition. However, the correlation framework of the E member indicates the early establishment of a relatively large (Table 1) yet confined depocentre, filled in with a sheet-like succession composed of sand-rich clusters of thick-bedded turbidites intercalated with few m to few tens of m-thick packages of thin bedded turbidites (Carruba et al. 2004; Felletti et al. 2009). Isopach maps and basin-scale correlations of the E member hint at a gradual decrease in the gradient of the basinal slopes, suggesting that the degree of confinement of its turbidite systems might have reduced swiftly because of infilling from turbidites. The sand-rich thick-bedded component of the E member includes two main turbidite types: i) T_a-missing or complete *Bouma* sequence turbidites (few tens of cm to less than c. 190 cm), interpreted as the product of waning surge-like flows, and ii) very thick beds and megabeds (thickness in range of c. 270-1200 cm) with massive bases which grade upward into thick laminated intervals with repeated sequences of sedimentary structures. Typically, the latter bed type is capped by thick mud caps which, together with the well structured character of the sandstone below suggest deposition from long-lived turbidity currents ponded by the basin topography (Felletti et al. 2009, *cf.* with 'contained beds' of Pickering and Hiscott, 1985). These two types of thick-bedded turbidite show contrasting bed planforms as well, with *Bouma*-like turbidites tapering distally and being generally smaller than the receiving depocentre as opposed to beds with a ponded character being tabular and basin-wide (Felletti et al. 2009). The thin-bedded component of the E member constitutes a significant fraction of the stratigraphy (c. 25 % of the total thickness) and includes both T_{cd} *Bouma* sequence turbidites starting with a basal sand and way more numerous cm-thick silty turbidites (T_d *Bouma* divisions) locally intercalated with hemipelagites. Although all of the bed types are ubiquitous in the studied section, there is a stratigraphic trend toward reduction of both the thickness of 'ponded' megabeds and typical ratio of mud cap to sandstone thickness of event beds from the lower to the upper half of the E member (**CL-1** and **CL-2**, respectively). Keeping with the geometry of the southern basinal slope (Carruba et al. 2004), this trend hints at a swift increase of the depocentre size as a result of sediment infilling and, possibly, onset of a late 'spill' phase in which a fraction of the finer grained part of larger incoming flows could escape the basin.

5. Results

5.1. Assessment of sampling biases affecting turbidite thickness statistics

In statistical analysis, a sample is a set of observations drawn from a population through a procedure devised to minimize sampling biases (Stuart, 1962). However, especially if the variable of interest is non-stationary in a xyz space and its population structure (including spatial trends) is unknown *a priori*, a random (or probability-based) sampling procedure cannot be trusted even when the number of samples is very large. In turbidite sedimentology spatial trends appear to be the rule rather than the exception, therefore a sound analysis of thickness statistics requires careful assessment of the following sources of sampling bias: i) a bed thickness dataset retrieved from a continuous section measured in a wellbore or in the field is representative of an interval of stratigraphic thickness z, which may contain turbidite systems with different sets of external controls; ii) in presence of spatial trends of turbidite thickness (e.g. laterally tapering beds related to stratigraphic pinch-outs, lobe shapes, channel fills), i.e. when thickness is non-stationary in xy, thickness data retrieved from a sampling location of given x, y coordinates can be biased toward or against certain thickness classes; iii) the number of thinner beds might be underestimated (see Drummond and Wilkinson, 1996) because thin bedded turbidites have a lower preservation potential of thicker beds due to erosion by subsequent flows or biogenic mottling (Weathercroft, 1990), they generally form shaly sections prone to cover from scree and vegetation and are impractical to detect even on good outcrops when they are finer-grained than coarse silt.

To get insights into the first sampling issue, turbidite thicknesses from the each of the three stratigraphic subsets of the Castagnola Fm, (**CS,** hereafter; see paragraphs 4.1 and 5.2.1) are plotted together with the full dataset of the same case study. The stratigraphic subsets of **CS** (**CS-1**, **CS-2**, and **CS-3** in Fig 6a) were defined by Marini et al. (2016) based on stratigraphic trends (i.e. changes in facies types, sand-to-mud ratio) which, with the support of independent observations on basin size, suggest different depositional processes and controls. It is therefore no surprise that the thickness statistics for these subsets and for the whole **CS** dataset are very different from each other (Figs 6a) and so do best-fitting results (Table 2).

The bias inherent to sampling location when a systematic spatial trend of thickness is present is illustrated in Fig 6b which compares data from two different correlative sections from the confined sheet-like Crognaleto lobe complex of the Laga Formation (**LF** hereafter; see paragraphs 4.3 and 5.2.3) at the basin centre and above the onlap onto the bounding slope. It can be noted that the thick-bedded tail of the subset from the onlap is shifted to the left compared to that of the basin centre, because the turbidites progressively thin approaching the slope (Fig 6b). In agreement with the overall sheet-like nature of the Crognaleto lobe complex, such bias toward thinner beds disappears when the sampling location moves away from the slope (*cf.* ‘off-centre’ with ‘centre’ in Fig 6b). Surprisingly enough, if two subsets c. 1 km apart from the laterally shifting lobes of the semi-confined Mt. Bilanciere lobe complex of **LF** (see paragraphs 4.3 and 5.2.3) are compared (Fig 6c), it is apparent that sampling location does not influence the shape of the curve. This can be explained by the memoryless and randomness nature of the compensational stacking of component beds of turbidite lobes (Mutti and Sonnino, 1981; Prelat and Hodgson, 2013), which makes two outcropping sections or boreholes not very far apart to intercept lobate geometries randomly, thereby resulting in similar empirical thickness distributions at the two locations if section thickness is at least several times larger than the average lobe thickness.

The modification of the 'true' frequency distribution of turbidite thicknesses arising from not detecting in the field the deposit of all of the flows entering a confined mini-basin is illustrated in Fig 6d-e using two simple yet meaningful experiments. Such experiments are grounded on the observation that, while bed correlatability between the two sections measured by Marini et al. (2016) c. 2.5 km apart is 100% for turbidites thicker than c. 10 cm, below this thickness threshold nearly 50% of the beds measured at one location cannot be identified at the other location. The reason for this correlation mismatching could be that because cm-thick turbidite sandstones typically have a basal grain size close to the limit between very fine sand and coarse silt, lateral fining of the deposit can make these beds difficult to identify across the whole basinal area. Alternatively, another possible explanation is that not all the very thin beds in the field could be identified because of usually poorer exposure of shale-prone thin bedded intervals. We anticipate here that best fitting of the **CS-1** subset suggests a log-normal model and an exponential model as plausible parent distributions for the full range of measured thickness ('all beds') and for the subpopulation of beds starting with a basal Tc or Td Bouma division, respectively (Table 2). In Fig 6d the subset of **CS-1** (378 beds) is plotted besides a synthetic dataset decimated of an arbitrary number of 150 very thin beds in order to simulate an enhanced effect of underdetection. The decimated dataset (228 beds) was generated by removing a percentage of the beds thinner than 10 cm from the full subset. The percentage of beds removed was higher for very thin beds (45% of beds <1 cm were removed), and diminished linearly up to a minimum of 5% for beds of 8-9 cm of thickness. Fig 6d illustrates that the underdetection of thin beds results in the down bending of the low-end tail and an increased upward convexity of the exceedance probability plot of **CS-1** and, presumably, in a modification of the parameters of the empirical distribution.

The experiment of Fig 6d assumes that the correlation mismatch documented in the nearby sections of the Castagnola Basin is due to lateral fining of the deposit and that in the field it was possible to measure the thickness of any deposit coarser than fine silts and therefore that **CS-1** represents the actual turbidite thickness population. However, if less than good exposition of shale-prone intervals were the reason for undersampling of thin beds, what we should have done in Fig 6d was adding, rather than subtracting such a fraction of beds as for Fig. 6e. Including a 'conservative' number of 150 undetected beds thinner than 10 cm results in the thin-bedded tail of the exceedance probability plot of **CS-1** to be visibly modified which, again, might be accompanied by a severe modification of the parameters of the empirical distribution(Fig. 6e).

Observations from the reported case studies show that in certain stratigraphic intervals thin beds are densely packed and form metre- to 10s metre-thick shale-prone packages (typical thin bed frequency is in order of 5 to 15 per metre). In these cases, an effect similar to that shown in Fig 6e can result from a short (less than 10 m) shaly interval of a stratigraphic section impossible to measure bed by bed for being intensely mottled due to bioturbation or covered.

5.2. Bed thickness statistics of the case studies

5.2.1. The Castagnola Formation (**CS**)

Exceedance probability plots suggest different statistical distributions for the three stratigraphic subsets ('all beds', black lines in Fig. 7a-c), with **CS-1** showing a very gentle upward convexity by way of a subtle gradient change across a thickness threshold of c. 30 cm, as opposed to the markedly convex upward shapes of **CS-2** and **CS-3** plots. Albeit any of these subsets fails to pass goodness-of-fit tests (Table 2), test statistics suggest a log-normal model as the best fitting choice. If thicknesses of **CS-1** turbidites are plotted as separate bed type subsets, we can note how the aforesaid gradient change corresponds to the breakpoint between the thin and thick bed subpopulations, which show no or negligible overlap. While best fitting results (Table 2) suggests that the first subset has been likely drawn from a population with an exponential distribution (cf. with Fig. 1), a power-law model turns out to be the best fit for the second subset, holding for more than a order of magnitude from 30 cm to up to c. 1100 cm. By comparing Fig. 7a and Fig. 7b is apparent how the mid-range part (thicknesses in range of c. 20 to 180 cm, see arrows in Fig. 7b) of the plot of **CS-2** has a quasi-linear trend similar to that of **CS-1**. Best fitting supports this observation (Table 2) yielding both apower-law and a log-normal models as plausible parent distributions for beds starting with a basal Ta/Tb division. This is accompanied with a noticeable down-bend of the plot of **CS-2** across a threshold at c.180 cm, meaning that the few beds in the high-end of the thickness population of **CS-2** are thinner than what is predicted is the power-law fit of Table 2 were to be preferred. Conversely, an exponential model represents the best fit (Table 2) for laminated to rippled beds of thickness less than c. 20 cm.

Lastly, the statistical distribution of turbidites from **CS-3** differs from those of the older units for showing no significant gradient break but a very smooth markedly convex upward shape on a log-log exceedance plot. If the two bed type subsets are considered separately, it can be noted how the two subpopulations of **CS-3** have overlapping thickness ranges. Fitting suggests an exponential and a log-normal model as likely parent distributions of the turbidites with a Tc/Td and a Ta/Tb and base, respectively.

Comparison of thicknesses across the three units (Fig. 7d) highlights the three stratigraphic subsets differ mostly for the length of their right thick-bedded tail and number of beds therein, with **CS-1** being much heavier-tailed than **CS-2** and **CS-3**. Such deficit of very thick beds in the two younger units is counterbalanced by higher frequencies in thickness classes in the range of 50 to 200 cm.

5.2.2. The Cengio (**CTS**) and Bric La Croce-Castelnuovo (**BCTS**) turbidite systems

Differently from previous works on these systems (Bersezio et al. 2005, 2009; Felletti and Bersezio 2010) only thickness measurements from the farthest locations available from basinal slopes are discussed in this paper, to avoid any location bias (see Section 5.1). The exceedance probability plots of thicknesses from both **CTS** and **BCTS** present an upward-convex character ('all beds', black line in Fig. 8a, b) resembling that of a log-normal or exponential distribution but very different from the linear trend typifying a power-law model (*cf* with Fig 1). Best-fitting suggests that **CTS** and **BCTS** subsets are both well described by a log-normal model (Table 2) with an exponential model as the second best fitting choice. Looking at Figs. 8a-b, a number of crossovers (black arrows) in the gradient of plots of both **CTS** and **BCTS** can be seen, corresponding from case to case to drops or increases in relative frequencies of beds in a given thickness range (i.e. between two steps). However, these steps would hardly make these empirical distributions to be mistaken as a 'segmented' power-law (see Malinverno, 1997 and Sylvester, 2007), given that any part of their log-log exceedance plots is not sufficiently straight to induce considering a power-law fit.

If thickness data are broken down into bed type subsets, it is apparent that the bed types subpopulations of both **CTS** and **BCTS** have overlapping thickness ranges, which can explain some of the observed steps of the plots (arrows in Fig. 8a-b) with a distribution mixing model (Talling, 2001; Sylvester, 2007; Pantopoulos et al., 2013). Shapes of exceedance probability plots and best fitting equally suggest that these bed subpopulations are all, again, well described by a log-normal model (Table 2). If thickness distributions of the two units are compared (Fig. 8c), it is apparent that they mainly differ in their thick-bedded tails (thickness greater than 100 cm), with beds in the thickness range of 100 to 400 cm being more numerous in **CTS**.

5.2.3. Laga Formation (**LG**)

The statistical distributions of turbidite thicknesses from each stratigraphic subset from **LG** (**LG-1** to **3**, from older to younger) are very similar to each other, showing convex-upward exceedance probability plots ('all beds' in Fig. 9a-c) and they all fit a log-normal model (Table 2). However, if bed type subsets are considered separately, some variability between different stratigraphic subsets can be observed. Best fitting indicates exponential and power-law behaviours for the turbidites of the confined **LG-1** with a Tc/Td and Ta/Tb and base, respectively, as opposed to a log-normal model for all bed type subsets of **LG-2** and **LG-3**. Also, if we focus on the very thick tails of the beds with a Ta/Tb base subset (thickness greater than c. 250 cm) it is noticeable how turbidites of **LG-1** and **LG-2** spread over a wider thickness range with respect to that of **LG-3** (Fig. 9a-c). This is better assessed contrasting thickness histograms (Fig. 9d), which suggest that from older to younger subsets, the thick-bedded tail of the distribution tends to be less 'heavy', i.e. misses an increasing number of beds thicker than the median thickness. Moreover, the heavier thick-bedded tail of **LG-2** with respect to that of **LG-3** is reflected in a greater value of σ of the log-normal best fit (i.e. the variance of the model distribution) and in a power-law model being the second best fit option (Table 2).

5.2.4. Cellino Formation (**CL**)

The exceedance probability plots of the lower (**CL-1**) and the upper (**CL-2**) E member of **CL** appear very different from those from other case studies. The curves have a segmented concave-upward shape between thicknesses of c.10 and 70 cm and a bi-partite thick-bedded tails (Figs. 10a, b). The convex-upward shape of plots Figs. 10a, b results from the high relative frequency of very thin silty turbidites that shift downward the low-end of the thicker-bedded part of the plots. If the thin-bedded tails of the two stratigraphic subsets are looked at into greater detail (see, for example, detail of Fig. 10c), it can be seen how the segmented character of their (Figs. 10a, b) might relate to mixing of subpopulations of turbidites deposited by flows with different character and having peculiar frequency distributions (see Talling, 2001; Sylvester, 2007; Pantopoulos et al., 2013), namely cm-thick silty T_d *Bouma* divisions (c. 80% of the thin-bedded subset), beds including a sandy rippled base (i.e. T_{cd} *Bouma* sequences) and complete or base-missing *Bouma* sequence turbidites.

As concerns the bi-partite nature of the thick-bedded tails of both **CL-1** and **CL-2**, Figs. 10a, b show that this is due a significant gap of thickness data (ranging from 190 to 270 cm as minimum) corresponding to the separation between non-ponded *Bouma* sequence turbidites and 'ponded' basin-wide megabeds (Fig. 10c). (Table 2). Considering the frequency distribution of 'ponded' turbidites only, both exceedance probability plots (Figs. 10a, b) and best-fitting results reveal some stratigraphic variability between the older more confined (**CL-1**) and the younger less confined (**CL-**

2). Indeed, while the thickness data of the **CL-1** plot almost as a line in Fig. 10a in agreement with a likely power-law fit (Table 2), those of **CL-2** describe a convex upward curve with a steeper high-end tail and are better fitted with a log-normal model.

6. Discussion

6.1. How can data collection procedures affect turbidite thickness statistics?

Most of the research on turbidite thickness frequency distribution has used the number of beds included in the analysis as a measure of significance of results. This prompted researchers to collate large datasets, including thickness measures from either thick stratigraphic intervals (Sylvester, 2007) or multiple, partly coeval sections logged in different parts of a basin (e.g. Talling 2001; Sinclair and Cowie, 2003; Felletti and Bersezio 2010). The results of paragraph 5.1 suggest that particular care must be placed in data collection to avoid biased representations of the actual thickness population. The example of the Castagnola Formation (Fig. 6a) illustrates that, though a large thickness dataset is desirable for adding significance to the statistical analysis, treating a thick study interval as a whole can result in thickness statistics that are considerably different from that of individual component units in case of the presence of stratigraphic trends. It is therefore important to assess any stratigraphic trend in the study interval prior to use turbidite thickness statistics as a tool for supporting process interpretations or predictions on reservoir architecture. The two examples from the Laga Formation (Figs. 6b, c) show that the choice of logging location can result in different empirical distributions across the basin, if turbidite thicknesses change laterally. Specifically, different empirical distributions are likely to occur where thickness is non-stationary in the xy space (i.e., bed geometry is not tabular) and subject to a systematic trend as a result of an external forcing such as, for example, the pinch-out of a turbidite bed set in the vicinity of basinal slopes of a confined basin (Figs. 6b). On the other hand, there is little influence on thickness statistics from location of the sampling site within unconfined laterally shifting lobes (Figs. 6c). This implies that while in presence of a systematic spatial trend (e.g. a stratigraphic pinch-out) the use of multiple correlative sections can result in a biased picture of thickness variability (*cf* 'centre+slope' with 'centre' and 'off-centre' plots in Fig 6b) and should therefore be avoided, in the case of turbidite beds with spatially random thickness variations it can provide a larger dataset with virtually no bias if the study section is sufficiently thick (*cf* 'all' plot with those of each of the different locations in Fig 6c). Finally, the experiments of Figs. 6d-e simulate the effect of undersampling of cm-thick turbidites with similar results to that of Malinverno (1997), and illustrates how even in an enclosed ponded mini-basin a considerable number of very thin depositional events are likely to be not detected also on fairly good outcrops. Further and even more severe sources of bias against thin beds include local erosion by subsequent flows (Drummond and Wilkinson, 1996; Sinclair and Cowie, 2003) and bioturbation (Weathercroft, 1990).

6.2. What are the implications of the bias against thin beds?

The under detection of the number of thin turbidite beds discussed in the previous section is particularly relevant when attempting to fit an empirical frequency distribution of turbidite thickness with existing model distributions. This is because, since turbidites typically show an inverse relationship between number of beds and thickness, the thin-bedded part of any empirical distribution is statistically so 'weighty' (e.g., in the studied datasets turbidites with thickness less than c. 30 cm typically represent more than 60% of the total number of beds) that it literally acts as a 'watershed' between alternative model distributions (e.g. log-normal vs. exponential and power-laws; see Fig. 1). The results of the experiments of Figs. 6d-e show how under detection of very thin beds can impact the low-end of empirical distributions, making for some ambiguity of fitting results not accompanied with an assessment of such type of bias. A quantification of the bias against thin beds resulting because or erosion by subsequent flows or, alternatively, biogenic mottling is provided by works by Kolmogorov (1951) and Muto (1995) which demonstrate that a significant part of the low-end tail of the actual bed thickness distribution may be not preserved in certain turbidite successions.

6.3. Stratigraphic variability of the thick-bedded tails of the case studies

After appraising likely biases related to data collection, we are now left with finding a way to compare the bed thickness statistics of different stratigraphic subsets and case studies. The sensitivity of the thin-bedded part of any turbidite thickness population to undersampling (see paragraphs 6.1 and 6.2), suggests that for an unbiased evaluation the focus should be on the reminder part of the thickness population. This could be done by either choosing a thickness cut-off, e.g. 10 cm, above which in good outcrop conditions it is reasonable to assume that all sandstone beds were detected or working with the thick-bedded subpopulation of the empirical datasets, namely that including only turbidites starting with a basal Ta/Tb *Bouma* division.

Here, the second approach is preferred because it restricts the treatment to the deposits of large volume turbidity currents that reached the measure location with similar initial rheology and were more likely to be confined by basin topography. Comparison of statistics (Fig. 11 and Table 3) of the thick-bedded tails of different stratigraphic subsets of a case study highlights a coherent modification of location and spread of the thickness population as a function of the degree of ponding. This modification consists in a decrease of the thickness quantiles greater than 50% (i.e. the median thickness) from older and more confined to younger and less confined stratigraphic subsets (Figs. 11a, c, e, g). In all of the case studies except for the Cellino Formation, this results in a likewise variation of mean, interquartile range and coefficient of variation values (Figs. 11b, d, f, h). The departure of the Cellino Formation subsets from this behaviour may be because the empirical samples are small (see Table 2) and include besides the ‘ponded’ beds, a significant but stratigraphically variable proportion (from 60% in the lower E member to 40% in the upper E member) of *Bouma* sequence turbidites. Restricting the treatment to ‘ponded’ beds only results indeed in these statistics to conform to the aforesaid trend (Figs. 11h). In addition, it is not surprising that the transition from the ponded to the partially ponded stage of the Castagnola Formation is accompanied by a subtle but opposite variation of the interquartile range (Figs. 11b), provided that the formulation of this statistical measure of dispersion does not account for either extreme values nor normalization to the mean of a distribution. Another way to look at the stratigraphic variability of thick-bedded tails is considering the high-end of both histograms and exceedance probability plots (see paragraph 5) which, from more confined to less confined units of the same case study, indicate a decrease in the frequency of thicker beds counterbalanced by an increase in frequency of mid-range thicknesses.

In summary, the observed variability points to an overall reduction of 'heaviness' of the high-end tail of thickness distributions (that is, how much it spreads toward high thickness values) from ponded (e.g. **CS-1**, **LG-1**, **CL-1**) or partially ponded/more confined systems (e.g. **CS-2**, **CTS** and **LG-2**) to less-confined (e.g. **BCTS**, **CL-1**) or unconfined systems (e.g. **CS3** and **LG-3**) of the same case study. It is suggested that sediment stripping and by-pass might represent the main controls on the 'heaviness' of the thick-bedded tail of turbidite thickness distributions of partially ponded to unconfined systems (see also paragraph 6.4 for additional discussion).

6.4. What model distribution best characterizes ponded turbidites?

If sampling biases were to be neglected, best-fitting results would suggest that, despite their diverse depositional controls, the frequency distribution of turbidite thickness from any of the case studies ('all beds' in Table 2) is reasonably well described with a log-normal model, though with some stratigraphic variability in statistical location and dispersion of data. However, acknowledging that a bias against very thin beds exists (see paragraphs 6.1-2) should lead to caution in drawing such a conclusion, provided that commonly applied scaling laws (i.e. exponential, log-normal and power-law) differ each from another in their low-end tail only (Talling, 2001; Sinlcair and Cowie, 2003; see also Cirillo, 2013).

As proposed in paragraph 6.3, a workaround to this problem is focusing on the thick bed subpopulations which, though not very numerous, have been shown to be less affected by sampling biases at the basin centre. If on one hand this approach may produce artificial truncation of the low-end tail of the thickness population, on the other hand it has the advantage of restricting the treatment to thick and laterally extensive turbidites deposited by large volume turbidity currents, that is, to those beds more likely to yield a depositional signature of flow confinement.

Results of distribution fitting of the thick bed subpopulations (Table 2) suggest that while the frequency distribution of thicknesses from ponded stratigraphic subsets (**CS1**, **LG-1** and **CL-1**) is better described by a power-law relationship, turbidite thickness data from partially ponded and confined to unconfined units from the same case studies show a log-normal behaviour. Admittedly, in most cases power-law and log normal models are very close best-fitting options (see Table 2), suggesting they are both plausible and that, though intriguing, our results are not definitive and need to be verified on larger thickness datasets via more refined approaches to goodness-of-fit testing. However, whichever the best distribution model for thick bed subsets of our ponded to partially ponded examples (i.e. power-law vs. log-normal with a high variance), the basin-wide character of these beds would imply that the volume of the sandy part of turbidity currents reaching the basin should scale linearly to turbidite thickness (Malinverno, 1997; Sinclair and Cowie, 2003) thus showing a likewise frequency distribution. This observation has important implications in prediction of net-to-gross in reservoir hosted in confined turbidite systems. Yet, it tells us little about the frequency distribution of parent flow magnitude, whose assessment would require taking into account the thickness of mud caps and is feasible only where there is a strong evidence of fully ponded conditions.

Should the power-law fit hold for the thick beds of our ponded to partially ponded examples, these basin-wide beds would represent the megabeds of the Malinverno (1997) model, namely the angular coefficient of the linear fits of Fig. 12 would represent $\beta_{mega.}$ However it is noteworthy that there is some variability in the scaling exponent β from smaller to larger basin, with the ponded examples from the Castangola and Laga formations (**CS-1** and **LG-1**) showing similar values ($\beta \approx 0.95$) much less than that of the power-law fit (β=1.54) of the Cellino Formation ponded subset (**CL-1**). While the variability of β is in general agreement with trivial calculations of scaling of bed volume to depocentre size, which predicts positive dependency of β on size of the basin given the same power-law input signal (see Sinclair and Cowie, 2003), dividing its value by that by the estimated average size of their host depocentre (Fig. 12) returns remarkably different values ranging from 0.013 of **CS-1** to 0.002 of **CL-1**. Also, it is unexpected finding that from smaller to larger depocentre there is an increase in average thickness (Table 3), suggesting that, overall, the thickness of these examples of ponded beds are positively related to depocentre size. There are two alternative explanations for these results: i) if a frequency distribution of parent flow magnitude with same scaling parameter β is to be assumed, our estimates of depocentre size might be significantly inaccurate, or ii) both the scaling parameter β and average magnitude of the input signal might be peculiar to each turbidite basin, e.g. depending on different dominant generative process and flow types (see Talling 2015 for a review) and character and size of source areas. Another interesting point highlighted by this study is that the ponded examples do not show any evidence of three well-defined thickness subpopulations with power-law behaviour nor of the corresponding gradients from β_{small} to β_{large} and β_{mega} predicted by the Malinverno (1997) model. Previously, Sylvester (2007) noted that the third segment β_{mega} had never been reported in the literature before his work, which in his view questions the possibility that the frequency distribution of volumes of turbidity currents might follow a power-law scaling relationship. Only more recently Felletti et al. (2009) and Felletti and Bersezio (2010) interpreted some cross-overs of the log-log exceedance probability plot of turbidite thickness as the transition between the three subpopulations of the Malinverno (1997) model but were not able to demonstrate the power-law behaviour of any of these subpopulations. Also, as the transition between the subpopulations of 'small' and 'large' beds were coupled with a change in facies types, the changes in plot gradient from β_{small} to β_{large} were interpreted by Felletti et al. (2009) and Felletti and Bersezio (2010) as primarily reflecting rheology transitions in parent flows rather than undersampling of beds of diameter smaller than the host basin radius.

However, reconsidering the assumptions of the Malinverno (1997) model, it must be noted that the two power-law subpopulations of 'small' and 'large' beds as well as the flex separating them on a log-log exceedance plot are not to be seen in the real world. This is because while the assumption of a cylindrical shape holds for ‘ponded’ beds (being basin-wide the planform of ‘ponded’ beds can be viewed as that of cylinder of diameter equal to that of the circular host basin) and will result in linear scaling of thickness to bed volume, the three-dimensional shape of the deposit of non-ponded or unconfined flows cannot be assumed to be unique and adequately described by a simple planform or scaling law of bed thickness to length and, therefore, the thickness of non-ponded beds might not follow a power-law frequency distribution even when volume of parent flows do so. In conclusion, any analysis of turbidite thickness statistics to identify the signal of basin confinement and flow ponding should be focused on the thick-bedded tail of the thickness distribution rather than on fitting the distribution of the whole thickness range to result of numerical models based on assumptions that might not be valid for the entire thickness range.

6.5. How is the initial bed thickness distribution modified by sediment by-pass?

What remains to be explored are the depositional controls behind the observed stratigraphic modification in all of the case studies from high-variance thickness populations having thick-bedded tails with likely power-law behaviour to low-variance thickness populations characterized by log-normal thick-bedded tails (Fig. 12 and 13).

Assuming that the input signal had not changed significantly over time, the plot of ponded subsets can used as the initial best representation of input volumes. If we focus on thick-bedded tails only for sake of better comparison (Fig. 13), this modification is expressed as an increase in the upward-convexity of the exceedance probability plot from older and more confined to younger and less confined stratigraphic subset.

Any explanation for the alterations of the initial thickness population shown in (Fig. 13) must account for the different mechanics of flow spilling (Sinclair and Tomasso, 2002) of partially ponded situations (e.g. **CS-2** and **LG-1** of the Castagnola and Laga formations) as opposed to sediment by-pass (see Stevenson, 2015 for a review) of open-end confined and unconfined turbidite systems. Also, it must take into consideration that, in ponded situations, the depocentre is progressively enlarging as it is filled up with turbidites (e.g., stratigraphic transition from **CS-1** to

CS-2 of the Castagnola Formation; see Table 1), which results in lateral shifting of the thickness exceedance probability plot.

The idealized plot of Fig. 14 is an attempt to summarize the results of this study into a comprehensive model tracking the likely modifications of the thickness frequency distribution of turbidites that are initially ponded in an enclosed mini-basin at a measured location close to the basin centre. As in the experiments of Malinverno (1997) and Sinclair and Cowie (2003), in initial stage 1, as nearly all turbidites are ponded and basin-wide, bed geometry can be approximated with cylindrical shapes of diameter equal to that of the depocentre.

The low-end of Fig. 14 plot below an arbitrary thickness of 20 cm is dashed showing that in stage 1 the initial frequency distribution of bed thickness (and that of magnitude of parent flows) below this threshold is unknown, and it could have followed a power-law model or had a log-normal behaviour and high-variance (Fig. 1). The plot focuses on how the initial thickness distribution is modified by depositional controls rather than its character and meaning. Also, the effect of increase of depocentre size is exaggerated to better visualize modifications of the initial distribution in four stages, from 1 to 4.

In stage 2 of Fig. 14, the depocentre enlarges and the height of the confining topography reduces as a consequence of sediment infilling (see Sinclair and Tomasso, 2002), There is an overall shift of the plot toward the left, signifying an overall decrease in location and spread (i.e. mean, range and variance) of the initial thickness frequency distribution and departure from its shape in both the thin and the thick-bedded tails. The down bend of the low-end of the plot can be viewed as the result of smaller flows being contained but not ponded by the depocentre topography: being their volume much less than the receiving depocentre, smaller flows neither develop a ponded character, nor deposit tabular basin-wide beds to be always intercepted in a section measured at the basin centre. This effect entails a drop in the frequency of low-end thicknesses reflecting undersampling of thin beds not reaching the measure location or too thin to be detected or preserved (see paragraph 6.1) and a thickness cut-off (stars in Fig. 14), scaling to the minimum volume of the flow able to develop a ponded character. This drop in the frequency distribution of thin beds is that same modelled by Malinverno (1997), being the only difference that in the real world, as these beds are not cylindrical but show diverse depositional shapes (and thickness frequency distributions) reflecting flow rheology transitions, the thin-bedded segment is likely to show a number of gradient changes (see e.g. Talling, 2001; Sylvester, 2007; Pantopoulos et al., 2013). The modification of the thick-bedded tail of stage 2 (Fig. 14) is interpreted as the result of onset of flow stripping in partially ponded conditions, that is, the height of the confining topography allows for some of the sand of the few largest flows to escape the basin spilling from a local sill. Differently from sediment by-pass in unconfined settings, flow stripping is selective with respect to flow magnitude (i.e. the amount of sediment escaping the basin is ultimately controlled the ratio of thickness of the flow to height of the confining topography) which makes for a sharp gradient change (circles in Fig. 14), or thickness cut-off, between the ‘ponded’ part of the plot and that subject to modification. Overall the above mentioned modifications of the initial distribution results in the plot of stage 2 showing a slightly convex-upward shape similar to that of empirical datasets of **CS-2** and **LG-1,** which both show a mild departure from the idealized plot of stage 1 in their thin and thick-bedded tails (Fig. 14a, c).

In stage 3 (Fig. 14), the severity of modifications addressed for stage 2 is increased as a result of the progress of depocentre infilling from turbidite. Is reasonable to assume that this might lead to ‘convergence’ of the thickness cut-offs of contained non-ponded turbidites and turbidites affected by flow stripping (arrows in Fig. 14) with the end result of well-defined convex-upward shape of the plot (e.g. **LG-2**; **CL-2**), which hints at a more that likely log-normality of the empirical distribution. Such a ‘convergence’ involves that establishment of flow ponding and scaling of bed thickness to parent flow volume is restricted to a progressively smaller range of flow magnitudes.

Stage 4 represents the situation where, further progression of depocentre evolution toward less confined situations, results in conditions unfavourable to ponding whichever the flow magnitude. The system is no longer ponded and none of the turbidite beds is basin-wide, therefore the frequency distribution of turbidite thickness does not scale linearly to flow magnitude but must be chiefly controlled by flow rheology, momentum and sediment by-pass. The model of stage 4 applies to all confined - non-ponded to unconfined examples of this study and is particularly well expressed in the **CTS** and **BCTS** (Fig. 14b), where there is a strong independent evidence of flow by-pass.

7. Conclusions

Aiming at assessing possible sampling biases and primary depositional control on turbidite thickness statistics of confined basins, in this study we compared a number of thickness subsets from four examples from the Central and Northern Apennine of Italy, which share a common stratigraphic evolution from an early ponded to a late unconfined depositional setting. The core finding of this research are as follows:

- A sound assessment of likely sampling biases is key to correct interpretation of turbidite thickness statistics, especially when spatial trends of bed thickness are documented. Sampling biases are lowest when thicknesses are measured at the basin centre, irrespective of the system internal architecture (basin-wide sheets pinching at basin margins vs. laterally shifting lobes).

- Stratigraphic variability in the studied succession should be accounted for by breaking down thickness datasets into subsets with homogeneous sedimentological characteristics in order to avoid a blurred statistical picture of turbidite thickness of little meaning for both process sedimentology interpretations and bed volume prediction.

- A bias against cm-thick Tc/Td *Bouma* sequence beds exists due to field operational constraints, which can lead to significant modifications of the actual thickness frequency distribution.

- The beds with a basal Ta/Tb deposited by larger volume flows form a high-end tail of the thickness population whose variance and frequency distribution bear some relationship to degree of flow confinement.
- Ponded examples where there is independent evidence of tabular basin-wide beds differ from non-ponded to unconfined examples of the same case study for showing a high-end tail of the thickness frequency distribution with higher variance and mean for which a power-law scaling law cannot be excluded based on our data.
- The frequency distribution of turbidite thicknesses measured at the basin centre in an initially ponded mini-basin can be modified higher in the stratigraphy to a lower-variance distribution because of flow-stripping and undersampling of thinner and laterally less continuous beds deposited by small-volume as a result of enlargement of the host basin and lowering of the height of the enclosing topography associated to basin infilling.

Acknowledgments

The Turbidites Research Group industry consortium (Anadarko, BG Group, BP, ConocoPhillips, Dana Petroleum, Nexen, OMV, Petronas, Statoil, Tullow Oil and Woodside) is warmly acknowledged for funding the research on the Castagnola Basin. Norske Shell AS and Statoil ASA are acknowledged for financially supporting past research on the Laga Basin. We gratefully acknowledge the reviewer George Pantopoulos for his constructive criticism and helpful comments which helped improving the clarity of the manuscript.

References

Awadallah, S.A.M., Hiscott, R.N., Bidgood, M., Crowther, T. 2001. Turbidite facies and bed-thickness haracteristics inferred from microresistivity images of Lower to Upper Pliocene rift-basin deposits, Woodlark Basin, offshore Papua New Guinea Eds P. Huchon, B. Taylor, A. Klaus, Proc. ODP, Sci. Results, 180, 1–30.

Baruffini, L., Cavalli, C., Papani, L. 1994. Detailed stratal correlation and stacking patterns of the Gremiasco and lower Castagnola turbidite systems, Tertiary Piedmont Basin, northwestern Italy. In: Weimer, P., Bouma, A.H., Perkins, B.F Eds 15th Annual Research Conference Submarine Fans and Turbidite Systems , Society of Economic Palaeontologists and Mineralogists, Gulf Coast Section, pp. 9-21.

Beattie, P.D., Dade, W.B., 1996. Is scaling in turbidite deposition consistent with forcing by earthquakes?: Journal of Sedimentary Research, v. 66, p. 909-915.

Bersezio, R., Felletti, F., Micucci, L., 2005. Statistical analysis of stratal patterns and facies changes at the terminations of ‘‘turbiditic’’ sandstone bodies: the Oligocene Cengio Unit Tertiary Piedmont Basin. GeoActa 4, 83–104.

Bersezio, R., Felletti, F., Riva, R, Micucci, L., 2009. Trends in bed thickness and facies of turbiditic sandstone bodies: unravelling the effects of basin confinement, depositional processes and modes of sediment supply. In: Kneller, B., Martinsen, O.J., McCaffrey, B. Eds., External Controls on Deep-Water Depositional Systems., vol. 92. SEPM Special Publications, pp. 303–324.

Boccaletti, M., Calamita, F., Deiana, G., Gelati, R., Massari, F., Moratti, G., Ricci Lucchi, F., 1990. Migrating foredeep-thrust belt system in the northern Apennines and Southern Alps. Palaeogeography, Palaeoclimatology, Palaeoecology 77, 3–14.

Bouma, A.H. 1962. Sedimentology of Some Flysch Deposits; A Graphic Approach to Facies Interpretation. Elsevier, Amsterdam, New York, 168 pp.

Carlson, J., Grotzinger, J.P., 2001. Submarine fan environment inferred from turbidite thickness distribution: Sedimentology, v. 48, p. 1331-1351.

Carminati, E., Doglioni, C., 2012. Alps vs. Apennines: The paradigm of a tectonically asymmetric Earth. Earth-Science Reviews 112 2012 67–96

Carruba, S., Casnedi, R., Felletti, F. 2004. From seismic to bed: surface–subsurface correlations within the turbiditic Cellino Formation central Italy.Petroleum Geoscience, 102, 131-140.

Carruba, S., Casnedi, R., Perotti, C. R., Tornaghi, M., Bolis, G. 2006. Tectonic and sedimentary evolution of the Lower Pliocene Periadriatic foredeep in Central Italy. International Journal of Earth Sciences, 954, 665-683.

Casnedi, R., 1983. Hydrocarbon-bearing submarine fan system of Cellino Formation, Central Italy: American Association of Petroleum Geologists Bulletin, v. 67, p. 359–370.

Casnedi, R., Follador, U., Moruzzi G., 1976. Geologia del campo gassifero di Cellino Abruzzo: Bollettino della Società Geologica Italiana, v. 95, p. 891-901.

Cavanna, F., Di Giulio, A., Galbiati, B., Mosna, S., Perotti, C. R. Pieri, M. 1989. Carta geologica dell'estremità orientale del Bacino Terziario Ligure-Piemontese. Atti Ticinesi di Scienze della Terra, 32.

Cazzola, C., Fonnesu, F., Mutti, E., Rampone, G., Sonnino, M., Vigna, B., 1981. Geometry and facies of small, fault-controlled deep-sea fan systems in a transgressive depositional setting. In: Ricci Lucchi, F. Ed.. IAS – 2nd European Regional Meeting Excursion Guidebook, Bologna, pp. 7–53 Tertiary Piedmont Basin, northwestern Italy.

Cazzola, C., Mutti, E., Vigna, B., 1985. Cengio Turbidite System, Italy. In: Bouma, A., Normark, W.R., Barnes, N.E. Eds., Submarine Fans and Related Turbidite Systems. Springer Verlag, pp. 179–183.

Centamore, E., Chiocchini, U., Cipriani, N., Deiana, G., Micarelli, A. 1978. Analisi dell’evoluzione tettonico-sedimentaria dei “bacini minori” torbiditici del Miocene medio-superiore nell’Appennino umbro-marchigiano e laziale-abruzzese: 5) risultati degli studi in corso. Memorie della Società Geologica Italiana, 18, 135-170.

Chen, C., Hiscott, R.N., 1999. Statistical analysis of facies clustering in submarine-fan turbidite successions. J. Sediment. Res. 69, 505–517.

Cirillo, P. 2013. Are your data really Pareto distributed?. Physica A: Statistical Mechanics and its Applications, 39223, 5947-5962.

Clauset, A., Shalizi, C. R., Newman, M. E. 2009. Power-law distributions in empirical data. SIAM review, 514, 661-703.

Di Giulio, A., Galbiati, B. 1998. Turbidite record of the motions along a crustal-scale tectonic line:the motions of the Villarvernia-Varzi line during the Oligocene-Miocene North-Western Italy. In: 15th Internetional Sedimentological Congress, pp. 293-294. IAS - Universidad de Alicante, Alicante, Spain.

Doglioni, C., 1991. A proposal of kinematic modelling for W-dipping subductions – possible applications to the Tyrrhenian–Apennines system. Terra Nova 3, 423–434

Drummond C.N., 1999. Bed-thickness structure of multi-sourced ramp turbidites: Devonian Brailler formation, Central Appalachian Basin: Journal of Sedimentary Research, v. 69, p. 115-121.

Drummond, C.N. and Wilkinson, B.H., 1996. Stratal Thickness Frequencies and the Prevalence of Orderedness in Stratigraphic Sequences: Journal of Geology, v.104, p. 1-18.

Felletti F., Carruba S. and Casnedi R. 2009. Sustained turbidity currents: evidence from the Pliocene Periadriatic foredeep Cellino Basin, Central Italy. In Kneller, B., Martinsen, O.J., and McCaffrey, B., eds., External Controls on Deep-Water Depositional Systems: SEPM Special Publication 92, 325-346.

Felletti, F., 2002. Complex bedding geometries and facies associations of the turbiditic fill of a confined basin in a transpressive setting (Castagnola Formation, Tertiary Piedmont Basin, NW Italy). Sedimentology 49, 645–667.

Felletti, F. 2016. Depositional architecture of a confined, sand-rich submarine system: the Bric la Croce – Castelnuovo turbidite system (Tertiary Piedmont Basin, Oligocene, NW Italy). Italian Journal of Geoscience, 134 (2015). DOI: 10.3301/IJG.2015.15

Felletti, F., Bersezio, R., 2010. Quantification of the degree of confinement of a turbidite-filled basin: a statistical approach based on bed thickness distribution. Mar. Pet. Geol. 27, 515e532.

Flint, S.,Bryant, I.D. 1993. The geological modelling of hydrocarbon reservoirs and outcrop analogues. Int. Assoc. Sedimentol. Spec. Publ., 15, 269 pp.

Gelati, R., Gnaccolini, M., 1980. Significato dei corpi arenacei di conoide sottomarina Oligocene–Miocene inferiore nell'evoluzione tettonico-sedimentaria del Bacino Terziario Ligure-Piemontese. Rivista Italiana di Paleontologia e Stratigrafia 87, 167–186.

Gelati, R., Gnaccolini, M., 1998. Synsedimentary tectonics and sedimentation in the Tertiary Piedmont Basin, Northwestern Italy. Rivista Italiana di Paleontologia e Stratigrafia 98, 425–452.

Ghibaudo, G., Massari, F., Chiambretti, I., d'Atri, A., 2014a. Oligo-Miocene tectono-sedimentary evolution of the Tertiary Piedmont Basin southern margin, Roccaverano area-Langhe sub-basin NW Italy. Journal of Mediterranena Earth Sciences, 6, 1-51.

Ghibaudo, G., Massari, F., Chiambretti, I., 2014b. Oligo-Miocene tectono-sedimentary evolution of the Langhe sub-basin: from continental to basinal setting Tertiary Piedmeont Basin – Northwestern Italy. Journal of Mediterranean Earth Sciences, 6, 53-144.

Goldstein, M.L., Morris, S.A., Yen, G.G. 2004. Problems with fitting to the power law distribution. Eur. Phys. J. B, 41, 255–258.

Haughton, P.D.W., 1994. Deposits of Deflected and Ponded Turbidity Currents, Sorbas Basin, Southeast Spain. Journal of Sedimentary Research Section, 642, 233-246.DOI: 10.1306/D4267D6B-2B26-11D7-8648000102C1865D

Haughton, P., Davis, C., McCaffrey, W., Barker, S., 2009. Hybrid sediment gravity flow deposits - Classification, origin and significance. Marine and Petroleum Geology, 2610, 1900-1918. DOI:10.1016/j.marpetgeo.2009.02.012 Hiscott, R. N.; Colella, A.; Pezard, P.; Lovell, M. A.;Malinverno, A. 1992. Sedimentology of deep-water volcaniclastics, Oligocene Izu-Bonin forearc basin, based on formation microscanner images. In Taylor, B., Fujioka, K., eds. Proc. Ocean Drilling Project, Scientific Results 126:75-96.

Hiscott, R.N., Colella, A., Pezard, P., Lovell, M.A., Malinverno, A., 1993. Basin plain turbidite succession of the Oligocene Izu-Bonin intraoceanic forearc basin. Mar. Petrol. Geol., 10, 450–466.

Isaaks, E. H.,Srivastava, R. M. 1989. Applied Geostatistics, 561 pp.

Janocko, M., 2010. Pinchout Geometry of Sheet-like Sandstone Beds: a new statistical approach to the problem of lateral bed thinning based on outcrop measurements. Lambert Academic Publishing. 978-3843380317.

Kolmogorov, A.N., 1951. Solution of a problem in probability theory connected with the problem of the mechanics of stratification. Ann. Maths Soc. Trans., 53, 171–177.

Kneller, B., McCaffrey, W., 1999. Depositional effects of flow nonuniformity and stratification within turbidity currents approaching a bounding slope; deflection, reflection, and facies variation. Journal of Sedimentary Research 695: 980-991.

Kneller, B.C., McCaffrey, W., 1999. Depositional effects of flow non-uniformity and stratification within turbidity currents approaching a bounding slope. Deflection, reflection and facies variation. J. Sediment. Res. 69, 980–991.

Lomas, S.A., Joseph, P., 2004. Confined turbidite systems. In: Lomas, S.A., Joseph, P. Eds., Confined Turbidite Systems. Geological Society, vol. 222. Special Publications, London, pp. 1–7.

Lowe, D. R. 1982. Sediment gravity flows: II Depositional models with special reference to the deposits of high-density turbidity currents. Journal of Sedimentary Research, 521.

Maino M., Decarlis A., Felletti F., Seno. S. 2013 – Tectono-sedimentary evolution of the Tertiary Piedmont Basin NW Italy within the Oligo–Miocene central Mediterranean geodynamics. Tectonics, Vol. 32, pp.1–27, doi:10.1002/tect.20047.

Manzi V., Lugli S., Ricci Lucchi F.,Roveri M. 2005 - Deep-water clastic evaporites deposition in the Messinian Adriatic foredeep Northern Apennines, Italy: did the Mediterranean ever dry out?. Sedimentology, 52, 875-902.Malinverno A., 1997, On the power-law distribution of turbidite beds: Basin Research. v. 9, p. 263-274.

Malinverno, A.,Ryan, W. B. 1986. Extension in the Tyrrhenian Sea and shortening in the Apennines as result of arc migration driven by sinking of the lithosphere. Tectonics, 52, 227-245.

Marini, M. Milli, S. Ravnås, R., Moscatelli, M. 2015. A comparative study of confined vs. semi-confined turbidite lobes from the Lower Messinian Laga Basin Central Apennines, Italy: Implications for assessment of reservoir architecture. Marine and Petroleum Geology 63, 142-165

Marini, M., Patacci, M., Felletti, F.,McCaffrey, W. D. 2016. Fill to spill stratigraphic evolution of a confined turbidite mini-basin succession, and its likely well bore expression: The Castagnola Fm, NW Italy. Marine and Petroleum Geology, 69, 94-111.

McBride, E. F. 1962. Flysch and associated beds of the Martinsburg Formation Ordovician, Central Appa-lachians. J. Sediment. Petrol. 32:39-91.

Milli, S., Moscatelli, M., Stanzione, O., Falcini, F., 2007. Sedimentology and physical stratigraphy of the Messinian turbidite deposits of the Laga basin central Apennines, Italy. Boll. Soc. Geol. Ital. 126, 255-281.

Milli, S., Moscatelli, M., Marini, M., Stanzione, O., 2009. The Messinian turbidites deposits of the Laga Basin Central Apennines, Italy. In: Northern and Central Apennines Turbidites Italy Edited By Tinterri R., Muzzi Magalhaes P., Milli S., Marini M., Moscatelli M., Stanzione O., Field Trip 12, 27th Ias Meeting 24-28 September 2009, Alghero, Italy, 35-54. ISBN 978-88-6025-123-7.

Milli, S., Cannata, D., Marini, M., Moscatelli, M., 2013. Facies and geometries of Lower Messinian Laga Basin turbidite deposits central Apennines, Italy. In: Milli S., Brandano M. Eds., Excursion Guidebook, post-congress field trip of the XI GeoSed congress, September 26-28, 2013. Journal of Mediterranean Earth Sciences, 5, 179-225.

Mizutani, S., Hattori, I. 1972 Stochastic analysis of bed thickness distribution of sediments. Math. Geol., 4, 123– 146.

Murray, C.J., Lowe, D.R., Graham, S.A., Martinez, P.A., Zeng, J., Carroll, A., Cox, R., Hendrix, M., Heubeck, C., Miller, D., Moxon, I.W., Sobel, E., Wendebourg, J., Williams, T., 1996. Statistical analysis of bed-thickness patterns in a turbidite section from the Great Valley Sequence, Cache Creek California. J. Sediment. Petrol 66, 900–908.

Mosca P., Polino R, Rogledi S., Rossi M. 2010. New data for the kinematic interpretation of the Alps–Apennines junction Northwestern Italy, Int J Earth Sci Geol Rundsch, V. 99, pp 833–849

Muto, T. 1995 The Kolmogorov model of bed-thickness distribution: an assessment based on numerical simulation and field data analysis. Terra Nova, 7, 417–423.

Mutti, E. 1992. Turbidite sandstones. Agip, Istituto di geologia, Università di Parma.

Mutti, E., Sonnino, M., 1981. Compensation cycles: a diagnostic feature of turbidite sandstone lobes, in: IAS Eur. Reg. Meeting, Bologna, Vol. Abstract II.

Pantopoulos, G., Vakalas, I., Maravelis, A., Zelilidis, A. 2013. Statistical analysis of turbidite bed thickness patterns from the Alpine fold and thrust belt of western and southeastern Greece. Sedimentary Geology, 294, 37-57.

Patacci, M., Haughton, P. D. W., McCaffrey, W. D. 2015. Flow Behavior of Ponded Turbidity Currents. Journal of Sedimentary Research 858: 885-902.

Patacci, M. 2016. A high-precision Jacob's staff with improved spatial accuracy and laser sighting capability. Sedimentary Geology 335: 66-69.

Pickering, K. T.,Hiscott, R. N. 1985. Contained reflected turbidity currents from the Middle Ordovician Cloridorme Formation, Quebec, Canada: an alternative to the antidune hypothesis. Sedimentology, 323, 373-394.

Pickering, K. T.,Hiscott, R. N., 2015. Deep marine systems: processes, deposits, environments, tectonics and sedimentation. John Wiley & Sons, 23 Oct 2015, 672 pp.

Prather, B. E., Pirmez, C., Winker, C. D. 2012. Stratigraphy of linked intraslope basins: Brazos-Trinity System, western Gulf of Mexico.Application of the Principles of Seismic Geomorphology to Continental-Slope and Base-of-Slope Systems: Case Studies from Seafloor and Near-Seafloor Analogues: SEPM Special Publication, 99, 83-109.

Prélat, A., Hodgson, D. M. 2013. The full range of turbidite bed thickness patterns in submarine lobes: controls and implications. Journal of the Geological Society, 1701, 209-214.

Ravnås, R., Steel, R. J. 1997. Contrasting styles of Late Jurassic syn-rift turbidite sedimentation: a comparative study of the Magnus and Oseberg areas, northern North Sea. Marine and Petroleum Geology, 144, 417-449.

Ravnås, R., Nøttvedt, A., Steel, R. J., Windelstad, J. 2000. Syn-rift sedimentary architectures in the Northern North Sea. Geological Society, London, Special Publications, 1671, 133-177.

Remacha, E., Fernández, L. P., Maestro, E. 2005. The transition between sheet-like lobe and basin-plain turbidites in the Hecho basin south-central Pyrenees, Spain. Journal of Sedimentary Research, 755, 798-819.

Ricci Lucchi, F. 1969. Channelized deposits in the middle Miocene flysch of Romagna Italy. Museo Geologico "Giovanni Capellini".

Ricci Lucchi, F., 1986, The Oligocene to Recent foreland basins of the northern Apennines: in Allen, P.,A., Homewood, P., eds, Foreland Basins Sp. Publ. of the IAS, v. 8, p. 105-139.

Ricci Lucchi, F. Valmori, E. 1980. Basin-wide turbidites in a Miocene, over-supplied deep-sea plain: a geometrical analysis. Sedimentology, 273, 241-270.

Rothman, D.H., Grotzinger, J.P. 1996 Scaling properties of gravity-driven sediments. Nonlinear Processes Geophys., 2, 178–185.

Rothman, D.H., Grotzinger, J.P., Flemings, P., 1994, Scaling in turbidite deposition: Journal of Sedimentary Research, v. 24, p. 59-67.

Sinclair, H. D. 1994. The influence of lateral basinal slopes on turbidite sedimentation in the Annot sandstones of SE France. Journal of Sedimentary Research, 641.

Sinclair, H. D., Tomasso, M. 2002. Depositional evolution of confined turbidite basins. J. Sediment. Res. 72:451-456.

Sinclair, H.D. Cowie, P.A. 2003 Basin-Floor Topography and the Scaling of Turbidites. J. Geol., 111, 277–299.

Southern, S. J., Patacci, M., Felletti, F. McCaffrey, W. D. 2015. Influence of flow containment and substrate entrainment upon sandy hybrid event beds containing a co-genetic mud-clast-rich division. Sedimentary Geology 321: 105-122.

Stevenson, C. J., Jackson, C. A. L., Hodgson, D. M., Hubbard, S. M., Eggenhuisen, J. T. 2015. Deep-water sediment bypass. Journal of Sedimentary Research, 859, 1058-1081.

Stocchi, S., Cavalli, C. Baruffini, L. 1992 I depositi torbiditici di Guaso Pirenei centro meridionali, Gremiasco e Castagnola settore orientale del BTP: geometria e correlazioni di dettaglio. Atti Ticinensi Scienze della Terra, 35, 154-177.

Stuart, A., 1962, Basic Ideas of Scientific Sampling, Hafner Publishing Company, New York.

Sylvester, Z., 2007, Turbidite bed thickness distributions: methods and pitfalls of analysis and modelling: Sedimentology, v. 54, p. 847–870.

Talling P., 2001, On the frequency distribution of turbidite thickness: Sedimentology, v. 48, p. 1297-1329.

Talling, P.J., 2013. Hybrid submarine flows comprising turbidity current and cohesive debris flow: deposits, theoretical and experimental analyses, and generalized models. Geosphere 9, 460–488.

Talling, P.J., Amy, L.A.,Wynn, R.B., Peakall, J., Robinson, M., 2004. Beds comprising debrite sandwiched within co-genetic turbidite: origin and widespread occurrence in distal depositional environments. Sedimentology 51, 163–194.

Tinterri, R. 2011. Combined flow sedimentary structures and the genetic link between sigmoidal-and hummocky-cross stratification.GeoActa, 104.

Tinterri, R., Tagliaferri, A. 2015. The syntectonic evolution of foredeep turbidites related to basin segmentation: Facies response to the increase in tectonic confinement Marnoso-arenacea Formation, Miocene, Northern Apennines, Italy. Marine and Petroleum Geology, 67, 81-110.

Lamb, M. P., Toniolo, H., Parker, G. 2006. Trapping of sustained turbidity currents by intraslope minibasins. Sedimentology, 531, 147-160.

Turcotte, D. L. 1997. Fractals and chaos in geology and geophysics. Cambridge, Cambridge University Press, 397 p.

Vai, G.B. 2001 Structure and stratigraphy: an overview. In Vai, G.B., Martini, I.P. eds Anatomy of an Orogen: the Apennines and Adjacent Mediterranean Basin, Kluwer Dordrecht, p.p. 15-32.

Van Andel, T. H., D Komar, P.. 1969. Ponded sediments of the Mid-Atlantic Ridge between 22 and 23 north latitude. Geological Society of America Bulletin, 807, 1163-1190.

Vezzani, L., Casnedi, R., Ghisetti, F., 1993, Geological map of the north-eastern Abruzzo region. Scale 1:100.000: S.EL.CA, Firenze.

Wheatcroft, R. A. 1990. Preservation potential of sedimentary event layers.Geology, 189, 843-845.

Figure and table captions

Table 1. Main characteristics of the case studies included in this work, compiled and partially revised from literature (see bottom row).

Table 2. Likely parent distributions for stratigraphic and bed type subsets with estimated parameters and results (rounded to two decimal places) of the Anderson-Darling (A-D) and Chi-Squared (Chi-Sq) goodness of fit tests. Thick marks in right-hand size of test statistics columns indicate that the model distribution passes the test with a significance level of 0.1whereas x indicate its rejection. 'Tc/Td base' and 'Ta/Tb base' bed type subsets are rippled to parallel laminated beds (i.e. Tc-d Bouma sequences) and beds starting with a massive or planar-parallel laminate division (i.e. Ta/Tb Bouma division).

Table 3. Descriptive statistics quantifying variability and location of the right thick-bedded tails of stratigraphic subsets from the case studies.

Figure 1. Log-log plot of thickness exceedance probabilities contrasting most commonly used model distributions for turbidite thicknesses: (1) power-law, (2) exponential and (3) low-variance log-normal and (4) high-variance log-normal model distributions. Note how the thick-bedded tails (right side of the plot) of 2 and 4 behave similarly to that of 3 and 1, respectively, making unpractical to distinguish between alternative model distributions when detailed data from the thin-bedded tail are not available.

Figure 2. Numerical experiments on turbidite thickness statistics of confined basins: (a) 'segmented' distribution of turbidite thicknesses measured at the centre of a circular basin produced using the assumptions of the 'confined basin model' of Malinverno (1997) (experiment 1, modified after Sylvester, 2007); (b) effects of (2) flow ponding and (3) flow stripping on thickness distributions of turbidites deposited in an enclosed circular basin by inbound flows with power-law volume distribution (1) (modified, after Sinclair and Cowie, 2003). See paragraph 2.1 for details and explanation.

Figure 3. Simplified sketch showing the eastward migration of the Apennine foredeep from Oligocene to present. Bold letters indicate turbidite infill of small, confined wedge top basins (**L**= Laga Basin; **C**= Cellino Basin). Modified after Di Biase and Mutti, 2002.

Figure 4. (a) Stratigraphic framework and (b) present-day layout of the Tertiary Piedmont Basin. Modified after Mosca et al. (2010).

Figure 5. (a) Stratigraphic framework of the Upper Miocene to Pleistocene deposits of the Laga Basin and the Periadriatic foreland system (modified after Carruba et al. 2006). Studied units in bold; (b) Simplified geological map of the Laga Formation and Cellino Formation outcrops with location of the composite sections from which thickness data were taken.

Figure 6. Bi-logarithmic thickness exceedance probability (as percent) plots showing a) the frequency distributions of turbidites from the individual stratigraphic units (**CS-1**, **CS-2** and **CS-3**) of the Castagnola Formation (**CS**) besides that of the whole **CS** dataset (**CS-1-3**); b) the

variability of the measured thickness distributions of a confined sheet-like turbidite package (Crognaleto lobe complex, Laga Formation) resulting from moving the measure location from the basin axis toward the lateral basinal slope; c) the variability of the measured thickness distributions of a package of turbidite lobes with compensational stacking (Mt. Bilanciere complex, Laga Formation) resulting from moving laterally the measure location; the effect of undersampling of cm-thick beds assuming **CS-1** (black line) as the actual bed thickness population (d) or (e) acknowledging that 150 beds thinner than 10 cm may have been not measured in the field. See text for explanation.

Figure 7. Turbidite thicknesses from the Castagnola Formation: (a), (b) and (c) are log-log exceedance probability plots of turbidite sandstone thicknesses from unit 1 to 3 with breakdown into bed type subsets; (d) is a histogram plotting the binned bed thicknesses, with the labels indicating the upper value of the bin interval, versus their relative frequency (logarithmic scale).

Figure 8. Turbidite thicknesses from the Cengio (CTS) and Bric la Croce-Castelnuovo Turbidite Systems (BCTS): (a) and (b) are log-log exceedance probability plots of turbidite sandstone thicknesses of CTS and BCTS, respectively, with breakdown into bed type subsets; (d) is a histogram plotting the binned bed thicknesses, with the labels indicating the upper value of the bin interval, versus their relative frequency (logarithmic scale).

Figure 9. Turbidite thicknesses from the lower Laga Formation lobes: (a), (b) and (c) log-log exceedance probability plots of turbidite sandstone thicknesses from the Poggioumbricchio (**LG-1**), the Crognaleto (**LG-2**) and the Mt. Bilanciere (**LG-3**) lobe complexes, respectively, with breakdown into bed type subsets; (d) histogram plotting bed thicknesses, with the labels indicating the upper value of the bin intervals, versus their relative frequency (logarithmic scale).

Figure 10. Turbidite thicknesses from the E member of the Cellino Formation: (a), (b) log-log exceedance probability plots of turbidite sandstone thicknesses from the lower (**CL-1**) and

more confined and the upper and less confined (**CL-2**) parts of the E member with breakdown into bed type subsets; c) detail showing the mixing of two further bed type subpopulation in the thin-bedded tail of **CL-1**; (d) histogram plotting bed thicknesses, with the labels indicating the upper value of the bin interval, versus their relative frequency (logarithmic scale).

Figure 11. Bar-charts of thickness quantiles (a, c and e, left-hand side) and mean, interquartile range (primary axes, in m) and coefficient of variation (dimensionless, on secondary axes) (b, d, and f, right-hand side) quantifying location and spread of the thick-bedded tail of stratigraphic subsets from (top to bottom) the Castagnola Formation, the Cengio-Bric la Croce-Castelnuovo Turbidite Systems, the Laga Formation lobes and E member of the Cellino Formation

Figure 12. Log-Log thickness exceedance probability plot comparing the thick-bed subpopulations of ponded examples from the Castagnola Formation (CS-1) Laga (LG-1) and Cellino (CL-1) formations. Note how the scaling parameter β increases from smaller to larger host depocentres in agreement with the model of Sinclair and Cowie (2003). Dashed lines are power-law best-fits of Table 2 noted with average estimated sizes of host depocentres.

Figure 13. Log-Log thickness exceedance probability plots comparing the frequency distributions of thick-bedded tails of stratigraphic subsets with different depositional controls (see legend) from: a) the Castagnola Formation, b) the Cengio-Bric la croce-Castelnuovo Turbidite systems, c) Laga Formation lobes and d) Cellino Formation Note how there is a tendency from more confined to less confined subsets to an increase in the overall upward-convexity of the plots relating to modification of shape and spread of thickness frequency distributions.

Figure 14. Log-Log thickness exceedance probability (as number of beds) plots showing the modifications affecting the empirical distribution of turbidite thicknesses at the basin centre of an enclosed ponded mini-basin were all of the turbidity currents are initially ponded (stage 1). Stage 2 and 3 illustrate the effect on the initial thickness distribution of progressive

enlargement of the depocentre and reduction of height of the confining topography with ongoing sediment infilling, resulting in smaller flows being no longer ponded by topography and few largest flows undergoing flow stripping. Stage 4 represents the final result of basin topography evolution, namely the onset of contained non-ponded or even unconfined conditions.

Figure 1

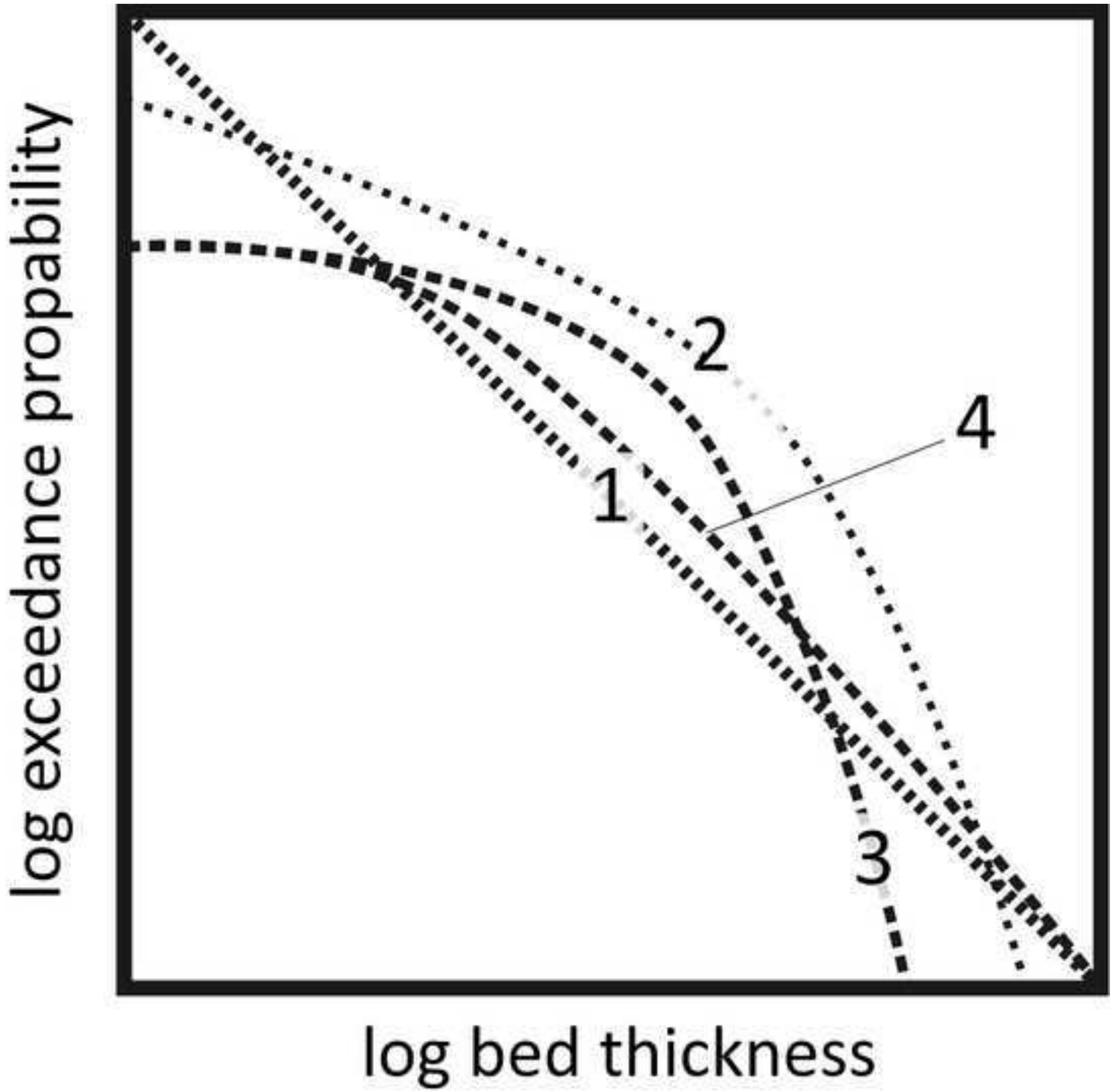

Figure 2

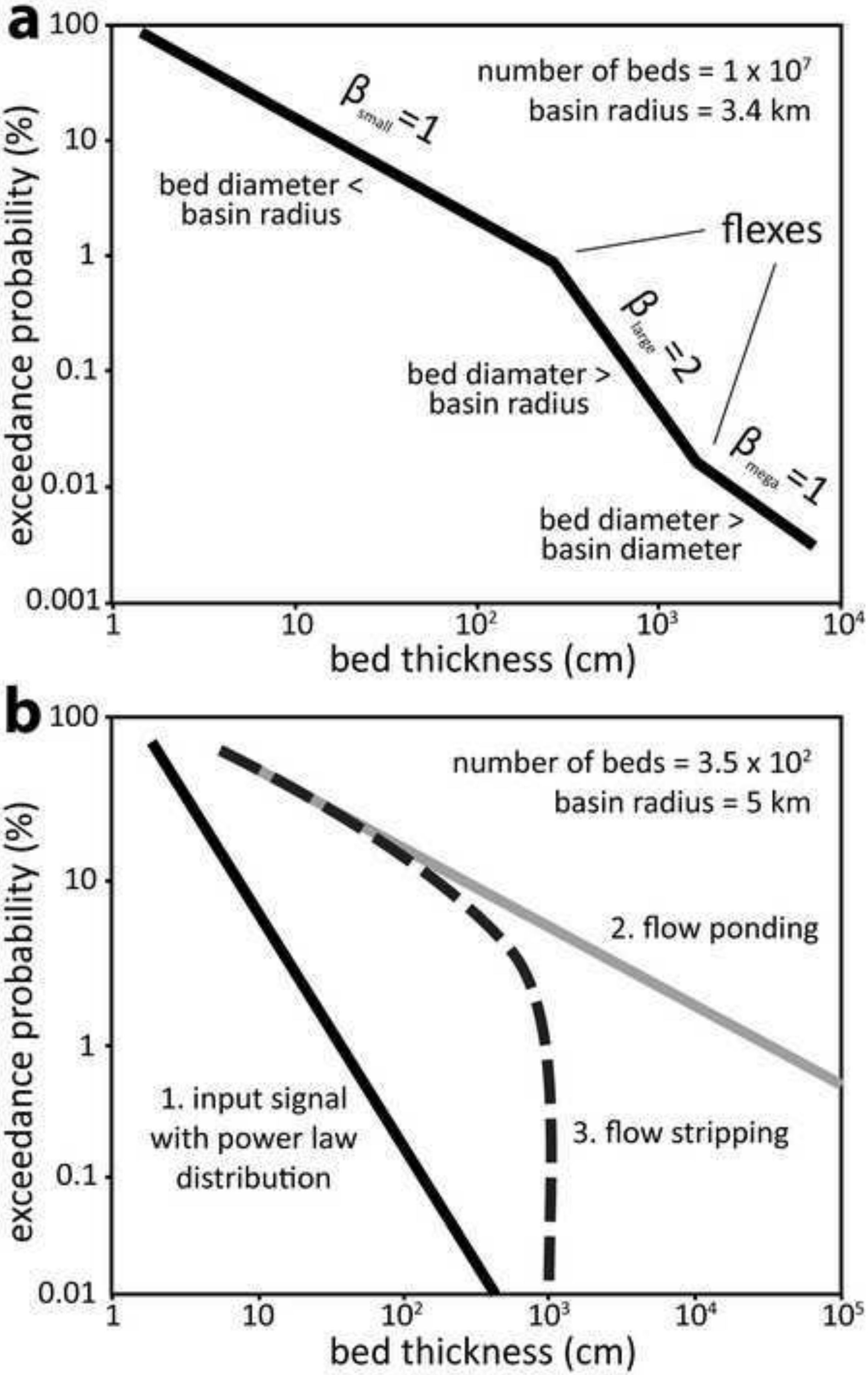
a
100
10
1
0.1
0.01
0.001
exceedance probability (%)
1
10
10²
10³
10⁴
bed thickness (cm)
number of beds = 1 x 10⁷
basin radius = 3.4 km
β small =1
bed diameter <
basin radius
flexes
β large =2
bed diamater >
basin radius
β mega =1
bed diameter >
basin diameter
b
100
10
1
0.1
0.01
exceedance probability (%)
1
10
10²
10³
10⁴
10⁵
bed thickness (cm)
number of beds = 3.5 x 10²
basin radius = 5 km
2. flow ponding
1. input signal
with power law
distribution
3. flow stripping

Figure 3

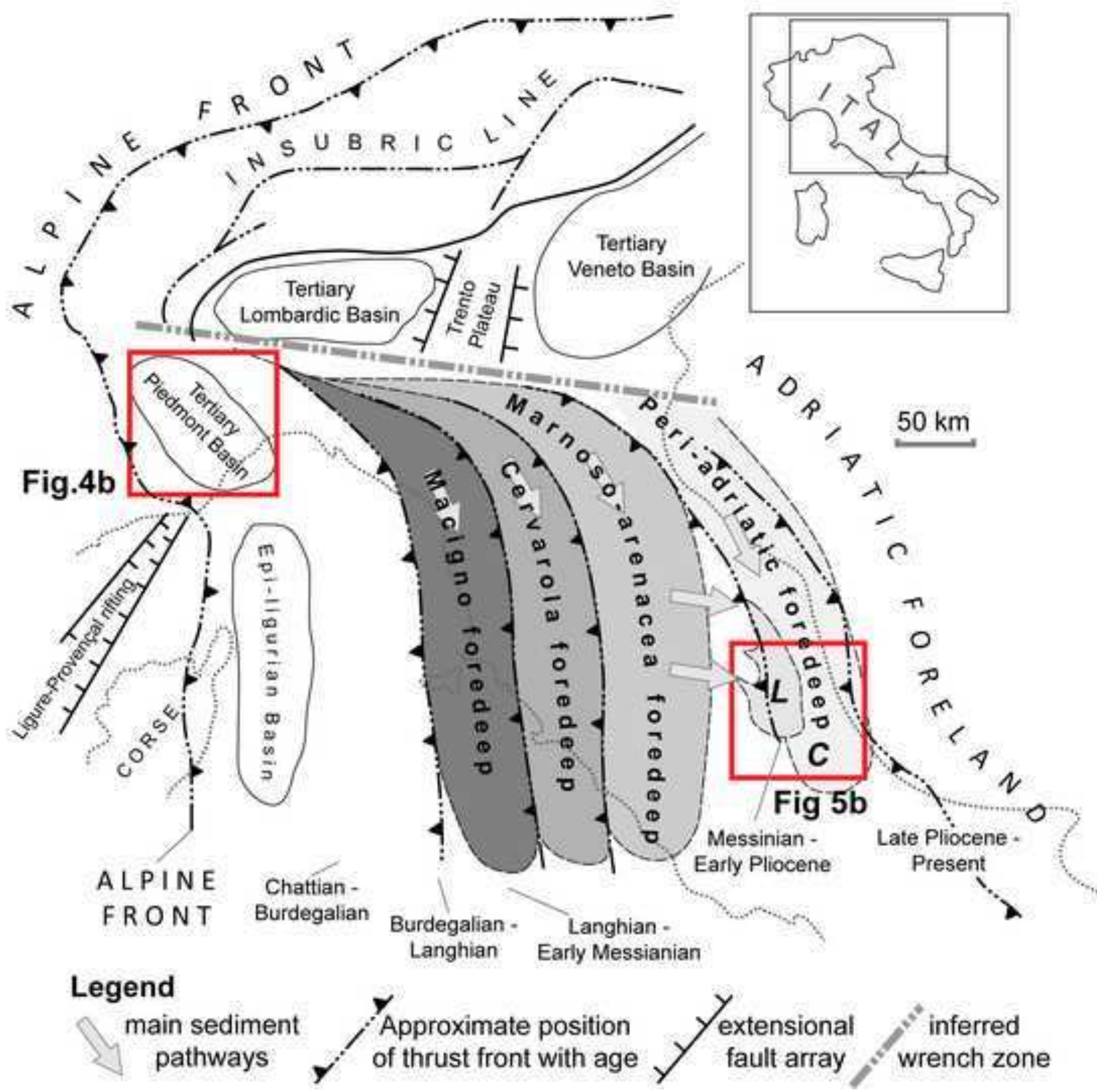
ALPINE FRONT
INSUBRIC LINE
Tertiary Lombardic Basin
Trento Plateau
Tertiary Veneto Basin
ITALY
ADRIATIC FORELAND
50 km
Tertiary Piedmont Basin
Fig.4b
Ligure-Provençal rifting
CORSE
Epi-ligurian Basin
Macigno foredeep
Cervarola foredeep
Marnoso-arenacea foredeep
Peri-adriatic foredeep
L
C
Fig 5b
ALPINE FRONT
Chattian - Burdegalian
Burdegalian - Langhian
Langhian - Early Messianian
Messinian - Early Pliocene
Late Pliocene - Present
Legend
main sediment pathways
Approximate position of thrust front with age
extensional fault array
inferred wrench zone

Figure 4

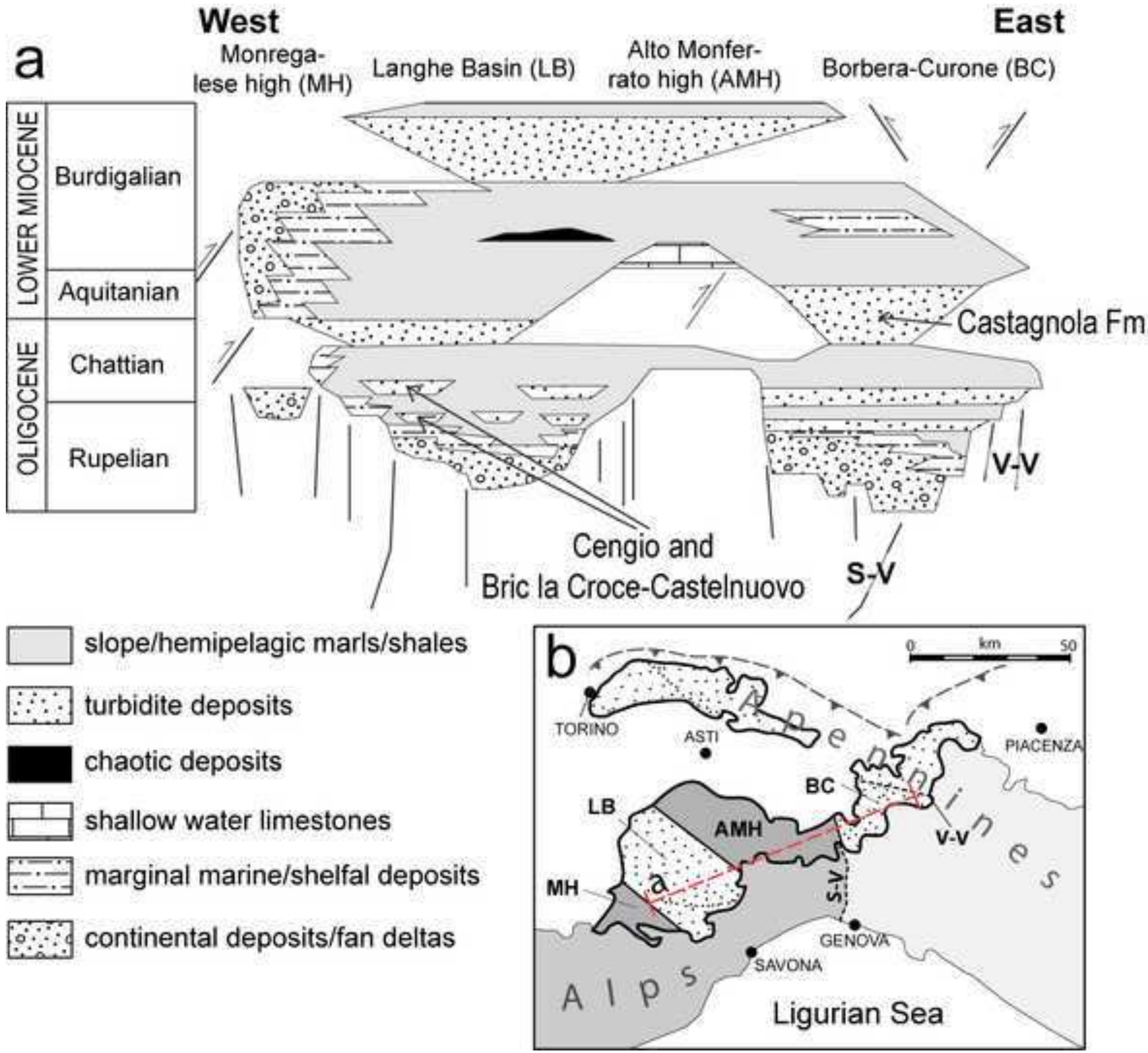
West
East
a
Monregalese high (MH)
Langhe Basin (LB)
Alto Monferrato high (AMH)
Borbera-Curone (BC)
LOWER MIOCENE
Burdigalian
Aquitanian
OLIGOCENE
Chattian
Rupelian
Castagnola Fm.
V-V
S-V
Cengio and
Bric la Croce-Castelnuovo
slope/hemipelagic marls/shales
turbidite deposits
chaotic deposits
shallow water limestones
marginal marine/shelfal deposits
continental deposits/fan deltas
b
0 km 50
TORINO
ASTI
PIACENZA
Apennines
BC
LB
AMH
V-V
MH
a
S-V
GENOVA
SAVONA
Alps
Ligurian Sea

Figure 5

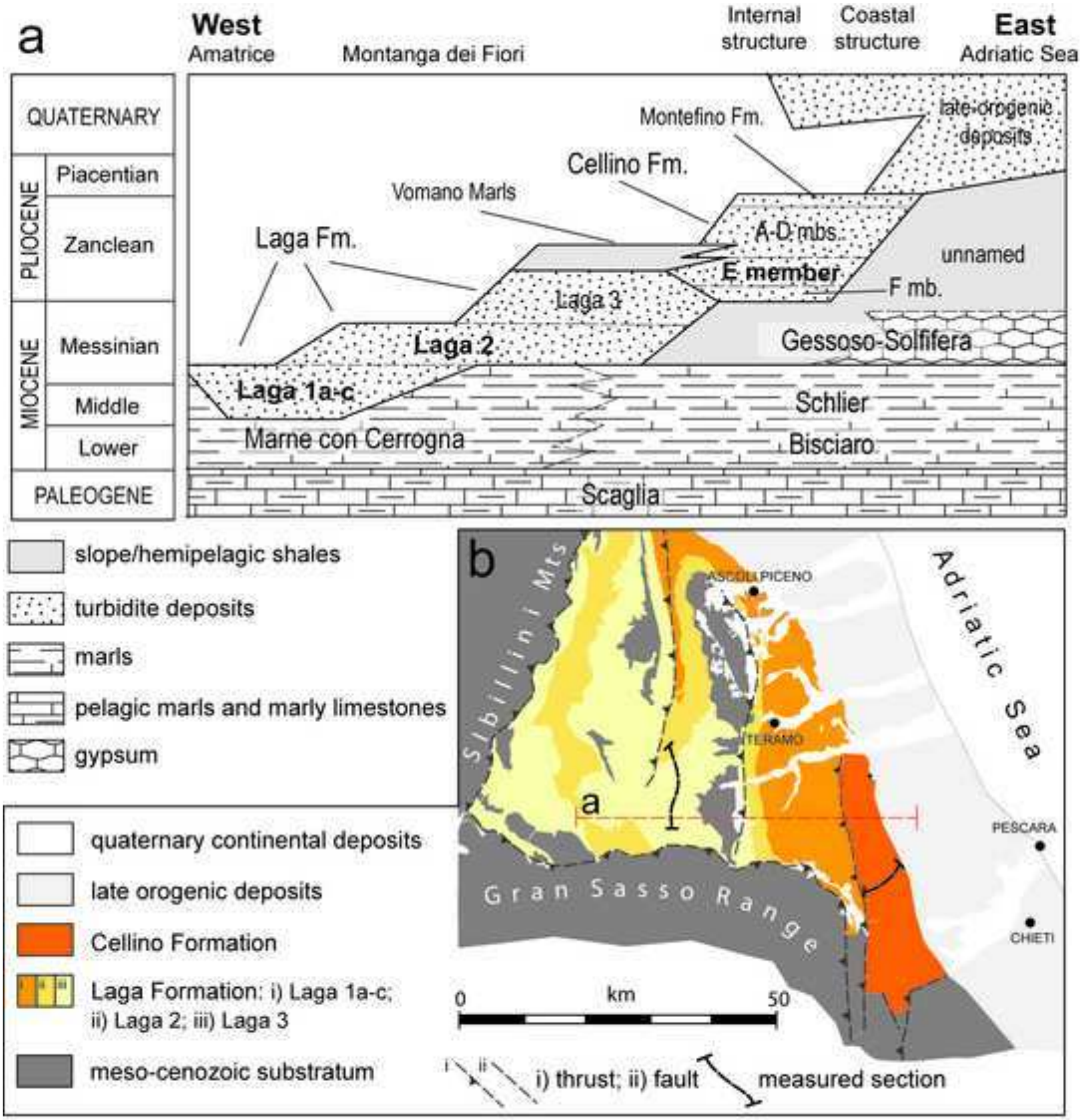

a
West
Amatrice
Montanga dei Fiori
Internal structure
Coastal structure
East
Adriatic Sea
QUATERNARY
PLIOCENE
Piacentian
Zanclean
MIOCENE
Messinian
Middle
Lower
PALEOGENE
late-orogenic deposits
Montefino Fm.
Cellino Fm.
Vomano Marls
Laga Fm.
A-D mbs.
E member
F mb.
unnamed
Laga 3
Laga 2
Gessoso-Solfifera
Laga 1a-c
Schlier
Marne con Cerrogna
Bisciaro
Scaglia
slope/hemipelagic shales
turbidite deposits
marls
pelagic marls and marly limestones
gypsum
b
Sibillini Mts
ASCOLI PICENO
Adriatic Sea
TERAMO
a
PESCARA
CHIETI
Gran Sasso Range
0
km
50
quaternary continental deposits
late orogenic deposits
Cellino Formation
Laga Formation: i) Laga 1a-c; ii) Laga 2; iii) Laga 3
meso-cenozoic substratum
i) thrust; ii) fault
measured section

Figure 6

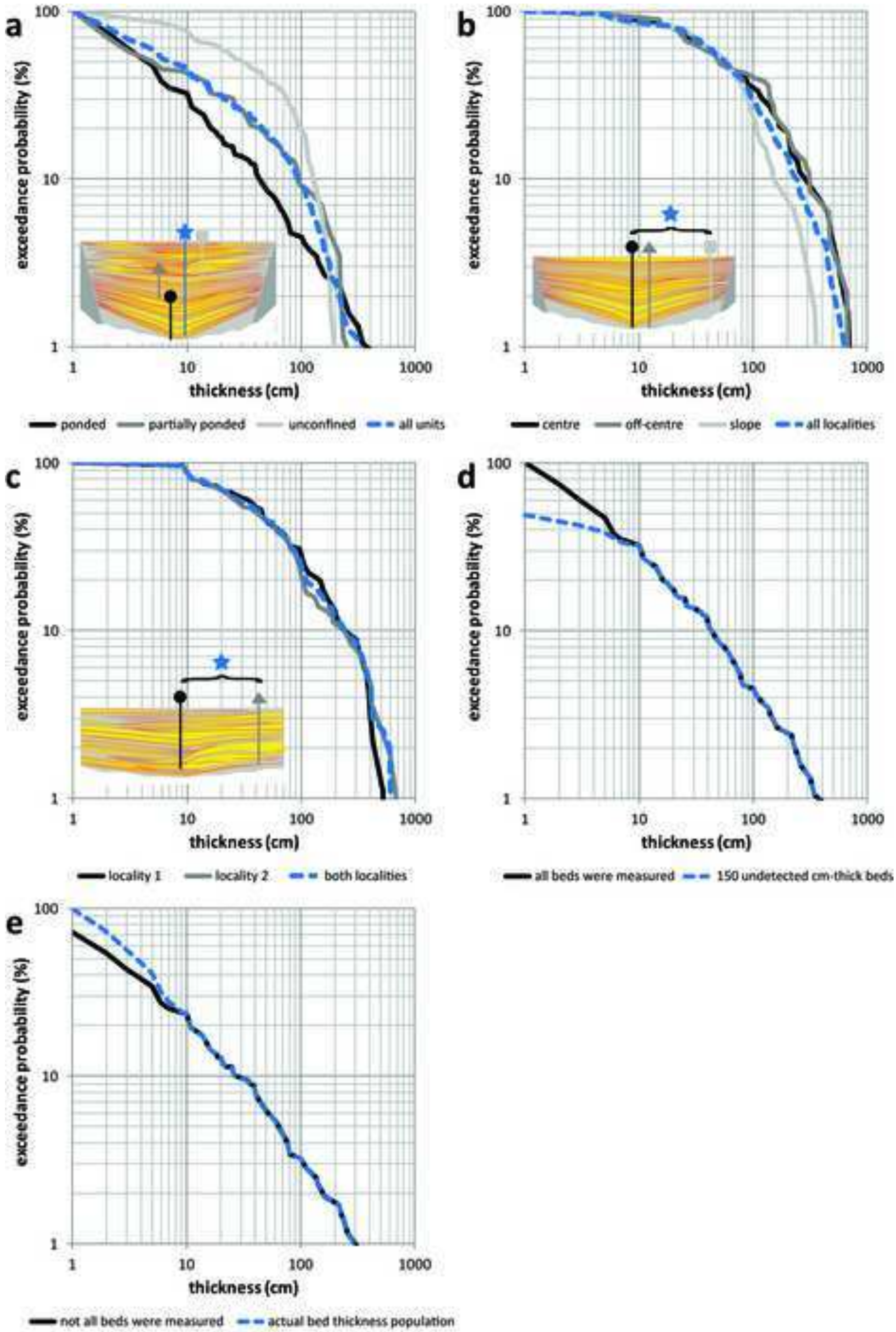
a
b
c
d
e
exceedance probability (%)
thickness (cm)
100
10
1
1
10
100
1000
ponded
partially ponded
unconfined
all units
centre
off-centre
slope
all localities
locality 1
locality 2
both localities
all beds were measured
150 undetected cm-thick beds
not all beds were measured
actual bed thickness population

Figure 7

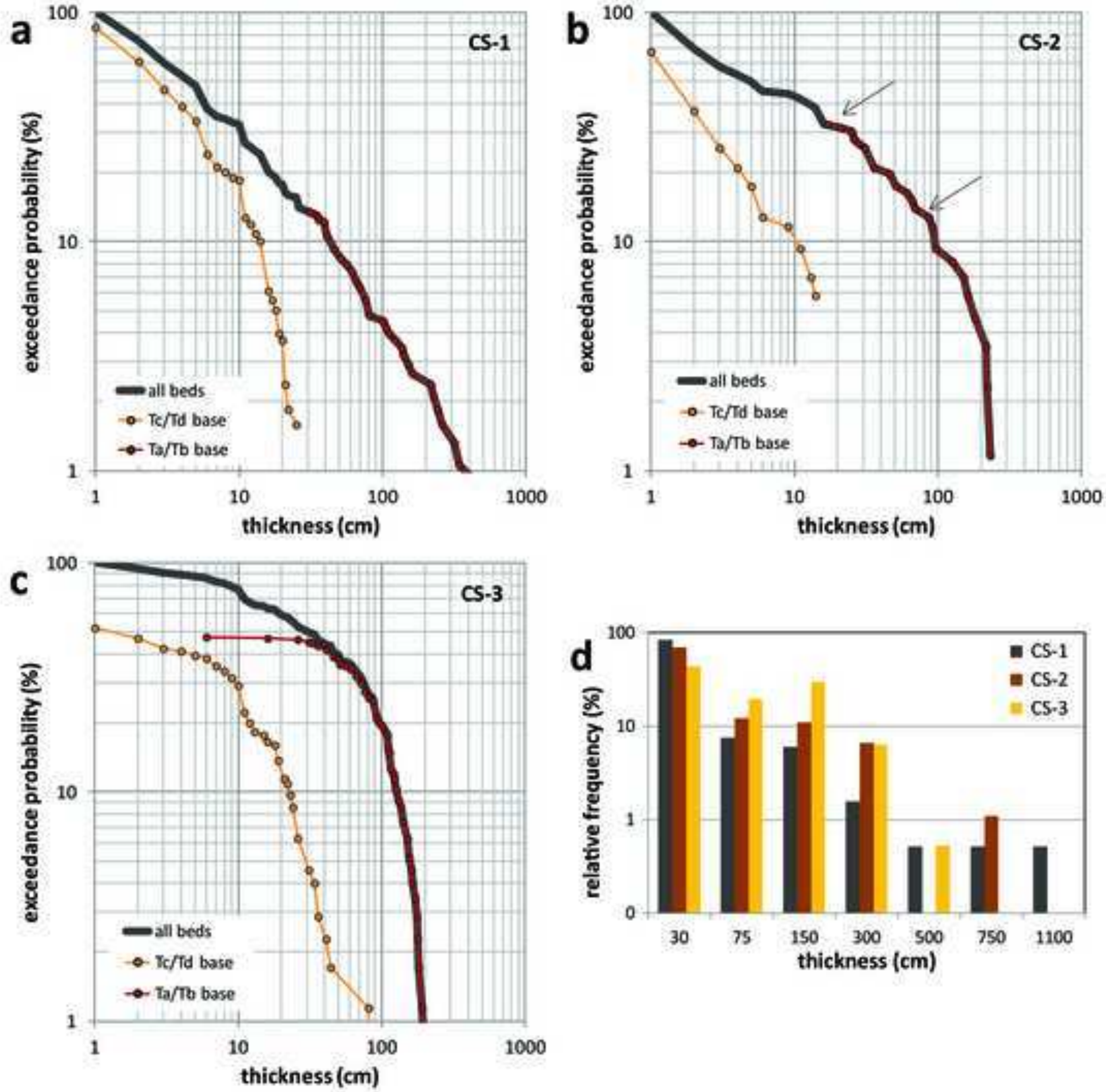
a
CS-1
exceedance probability (%)
thickness (cm)
all beds
Tc/Td base
Ta/Tb base
b
CS-2
exceedance probability (%)
thickness (cm)
all beds
Tc/Td base
Ta/Tb base
c
CS-3
exceedance probability (%)
thickness (cm)
all beds
Tc/Td base
Ta/Tb base
d
relative frequency (%)
thickness (cm)
CS-1
CS-2
CS-3
30
75
150
300
500
750
1100

Figure 8

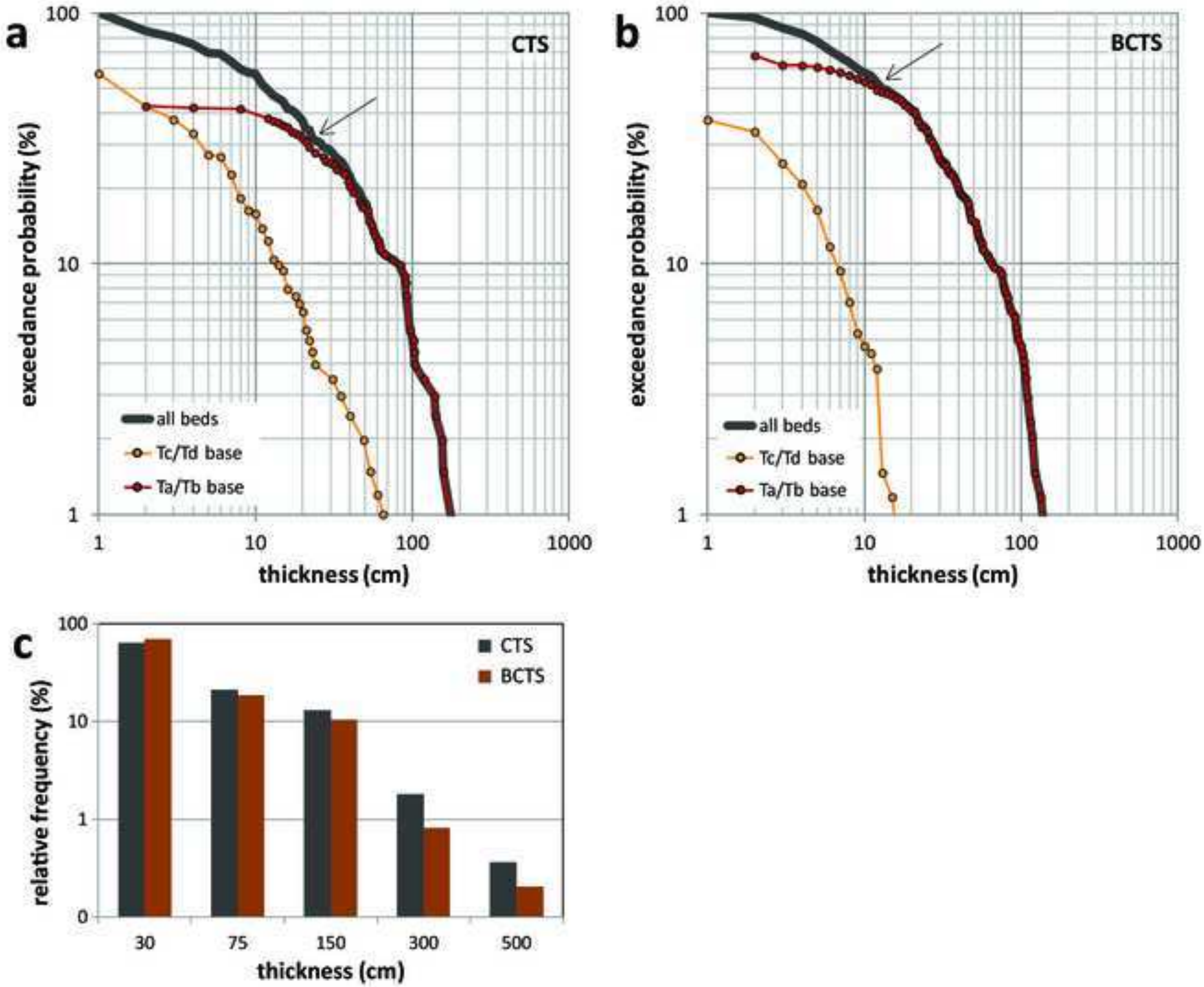

a
CTS
exceedance probability (%)
thickness (cm)
all beds
Tc/Td base
Ta/Tb base
b
BCTS
exceedance probability (%)
thickness (cm)
all beds
Tc/Td base
Ta/Tb base
c
CTS
BCTS
relative frequency (%)
thickness (cm)
30
75
150
300
500

Figure 9

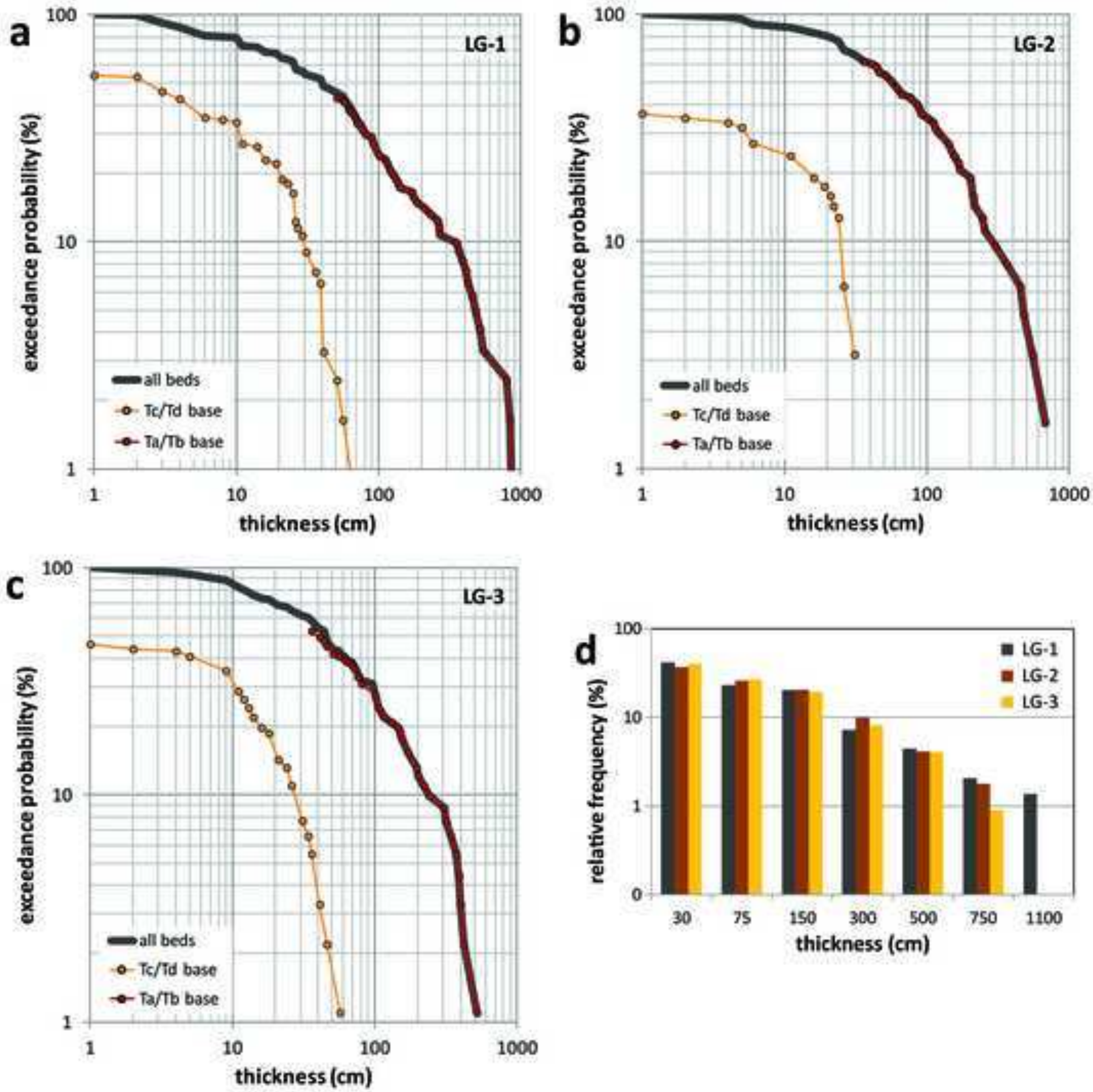
a
LG-1
exceedance probability (%)
thickness (cm)
all beds
Tc/Td base
Ta/Tb base
b
LG-2
c
LG-3
d
relative frequency (%)
LG-1
LG-2
LG-3
30
75
150
300
500
750
1100
thickness (cm)

Figure 10

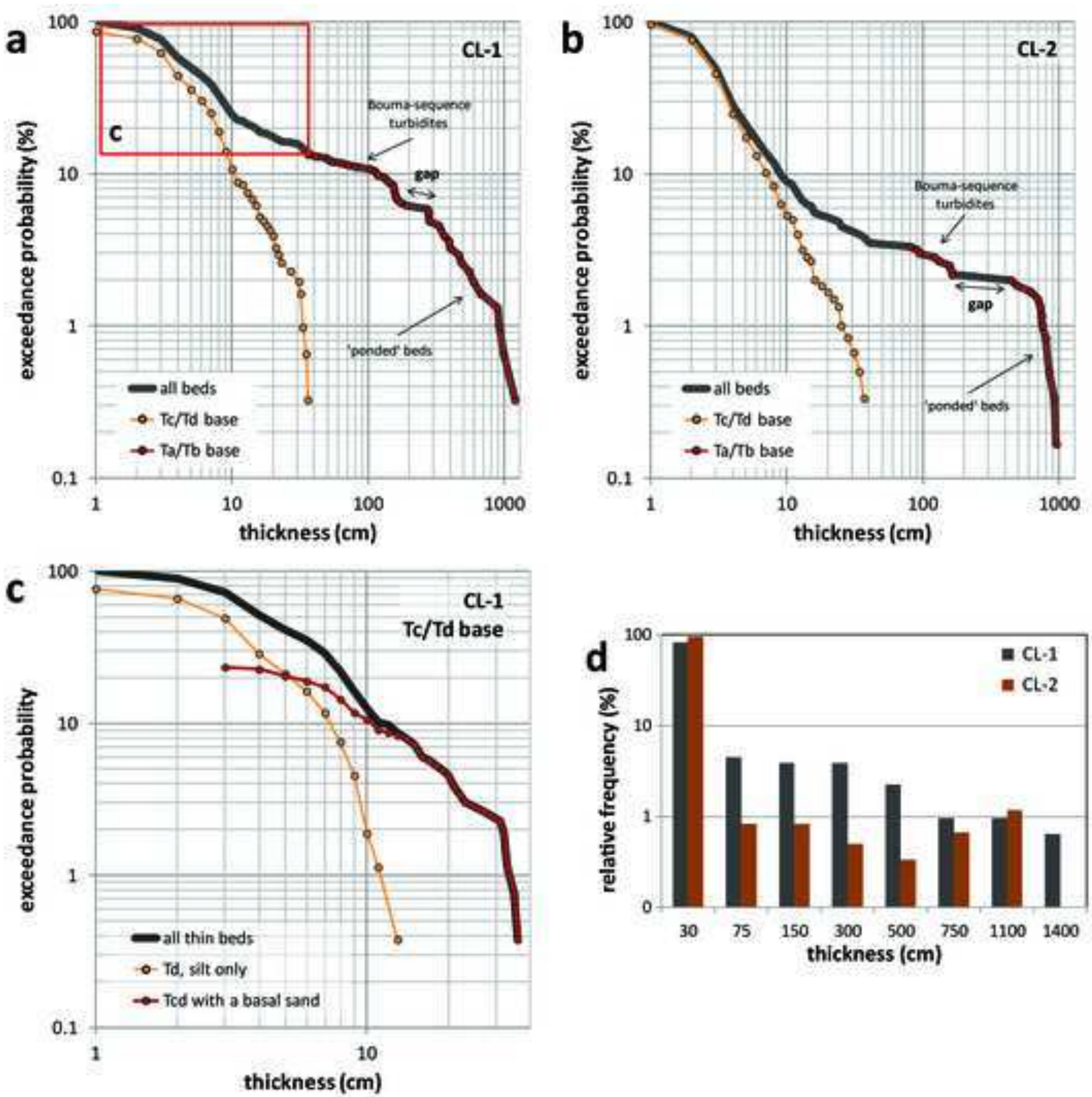

a
CL-1
c
Bouma-sequence turbidites
gap
'ponded' beds
all beds
Tc/Td base
Ta/Tb base
exceedance probability (%)
thickness (cm)
b
CL-2
Bouma-sequence turbidites
gap
'ponded' beds
all beds
Tc/Td base
Ta/Tb base
exceedance probability (%)
thickness (cm)
c
CL-1
Tc/Td base
all thin beds
Td, silt only
Tcd with a basal sand
exceedance probability
thickness (cm)
d
CL-1
CL-2
relative frequency (%)
30
75
150
300
500
750
1100
1400
thickness (cm)

Figure 11

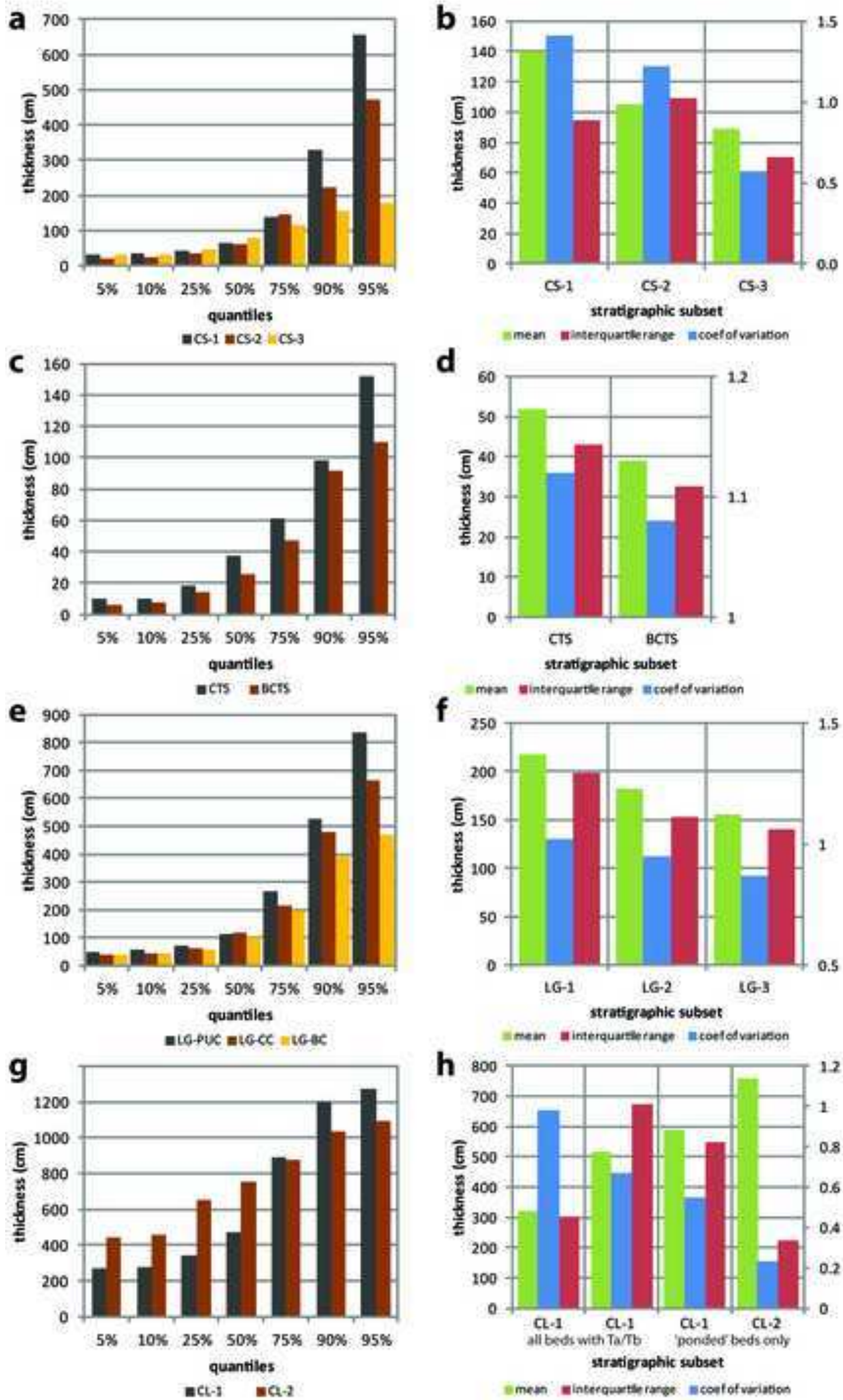
a
thickness (cm)
quantiles
5% 10% 25% 50% 75% 90% 95%
CS-1 CS-2 CS-3
b
thickness (cm)
CS-1 CS-2 CS-3
stratigraphic subset
mean interquartile range coef of variation
c
thickness (cm)
quantiles
CTS BCTS
d
thickness (cm)
CTS BCTS
stratigraphic subset
mean interquartile range coef of variation
e
thickness (cm)
quantiles
LG-PUC LG-CC LG-BC
f
thickness (cm)
LG-1 LG-2 LG-3
stratigraphic subset
mean interquartile range coef of variation
g
thickness (cm)
quantiles
CL-1 CL-2
h
thickness (cm)
CL-1 CL-1 CL-1 CL-2
all beds with Ta/Tb
'ponded' beds only
stratigraphic subset
mean interquartile range coef of variation

Figure 12

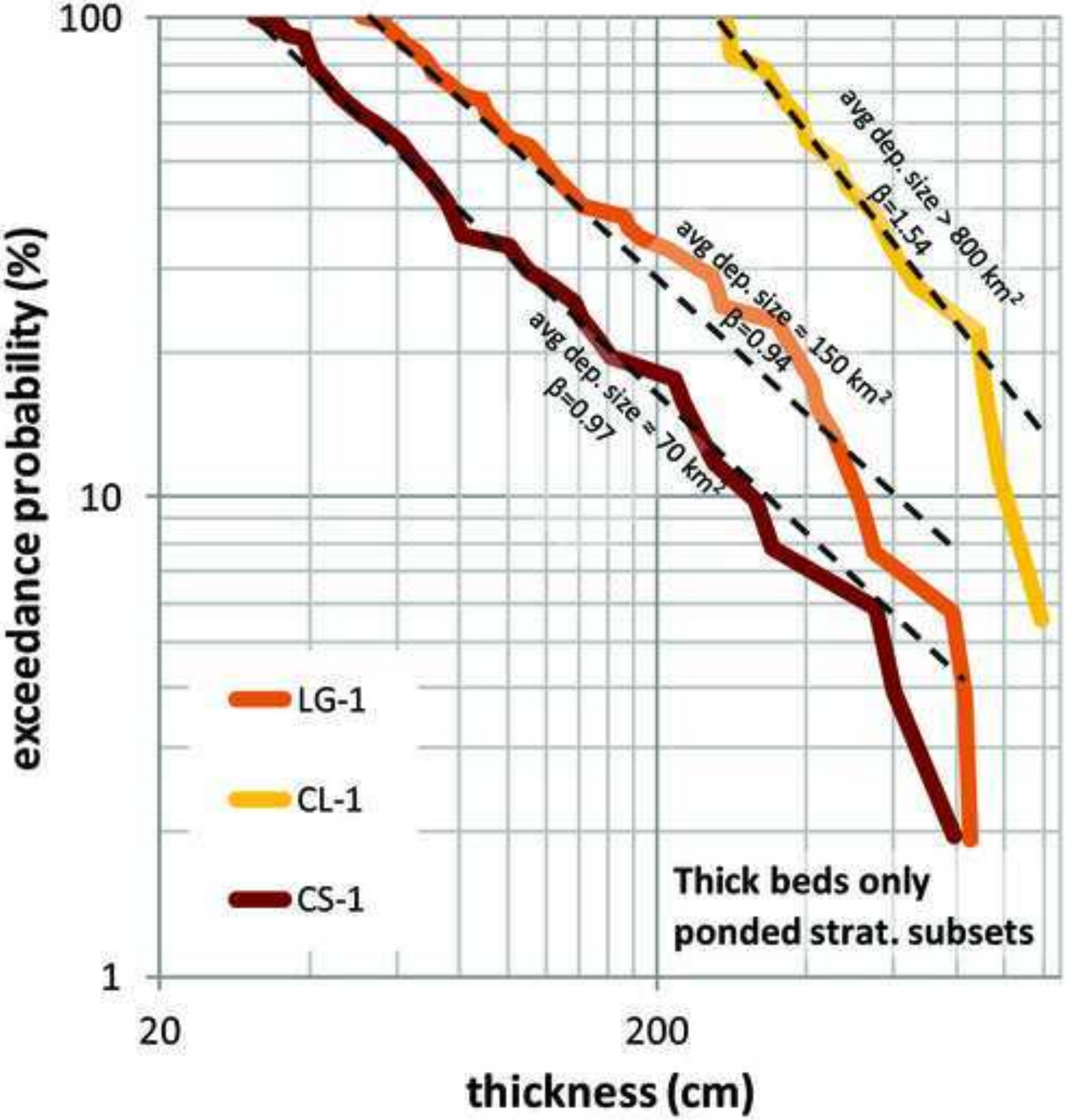

100
10
1
20
200
exceedance probability (%)
thickness (cm)
avg dep. size > 800 km²
β=1.54
avg dep. size ≈ 150 km²
β=0.94
avg dep. size ≈ 70 km²
β=0.97
LG-1
CL-1
CS-1
Thick beds only
ponded strat. subsets

Figure 13

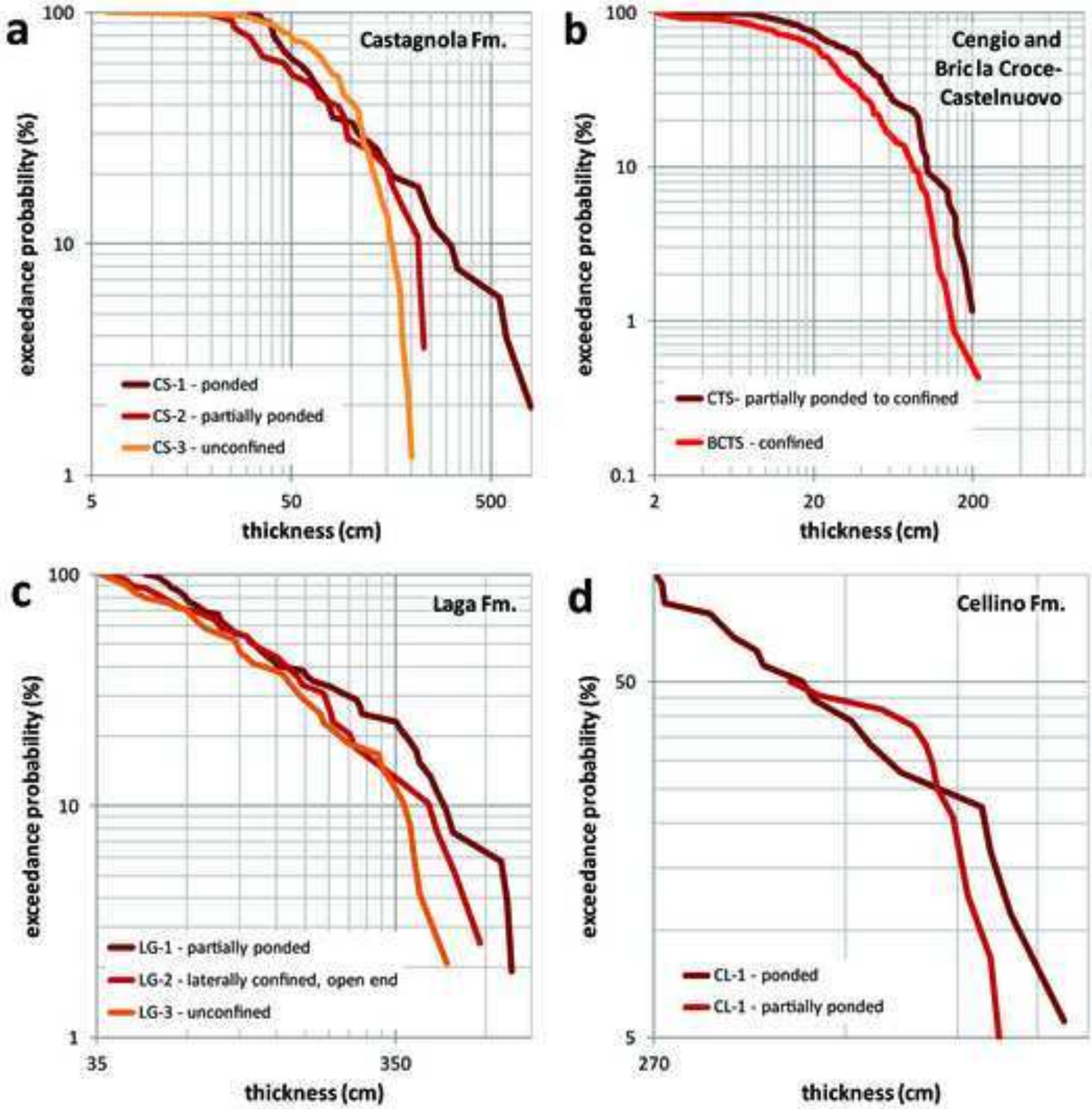

a
Castagnola Fm.
exceedance probability (%)
100
10
1
5
50
500
thickness (cm)
CS-1 - ponded
CS-2 - partially ponded
CS-3 - unconfined
b
Cengio and Bric la Croce-Castelnuovo
exceedance probability (%)
100
10
1
0.1
2
20
200
thickness (cm)
CTS- partially ponded to confined
BCTS - confined
c
Laga Fm.
exceedance probability (%)
100
10
1
35
350
thickness (cm)
LG-1 - partially ponded
LG-2 - laterally confined, open end
LG-3 - unconfined
d
Cellino Fm.
exceedance probability (%)
50
5
270
thickness (cm)
CL-1 - ponded
CL-1 - partially ponded

Figure 14

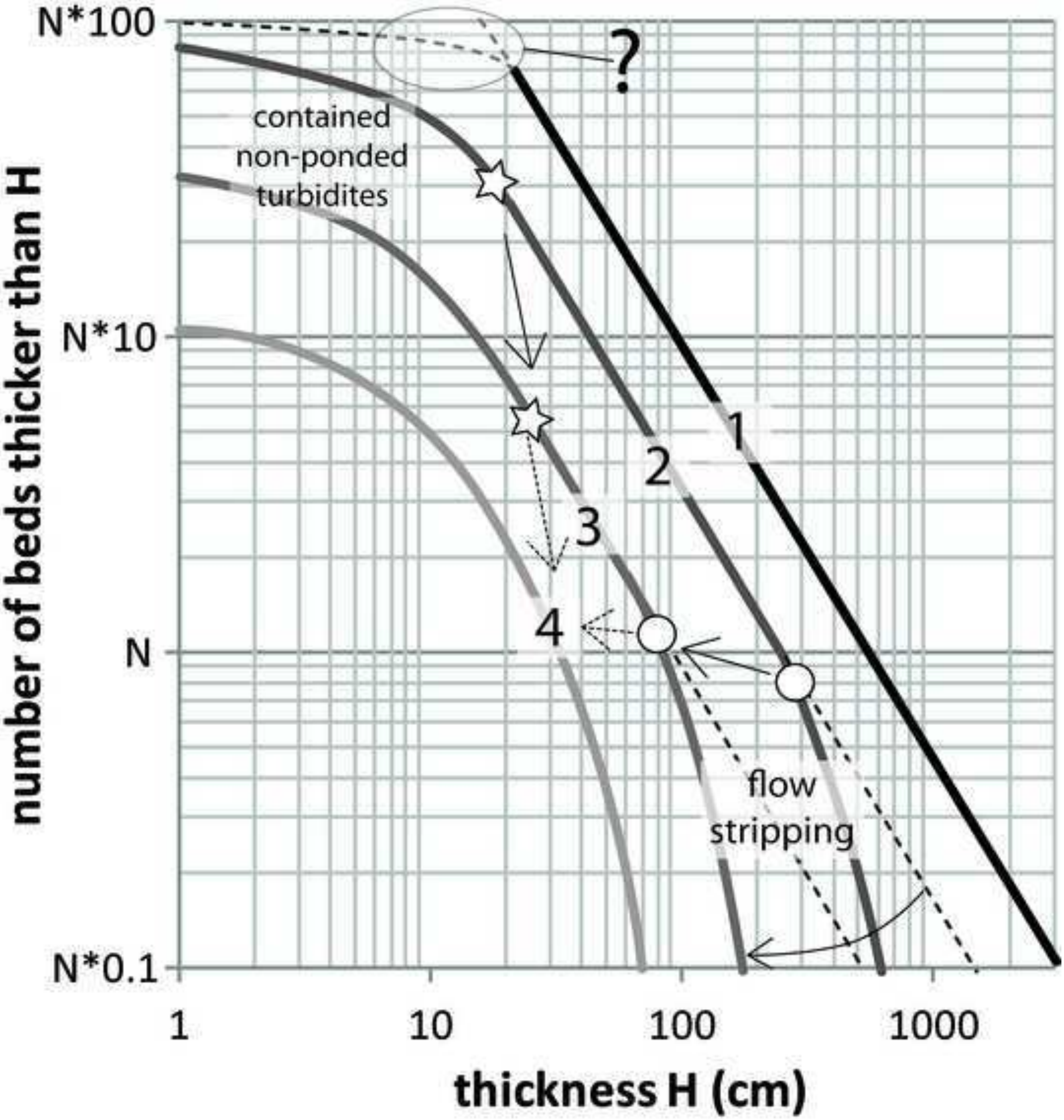

N*100
N*10
N
N*0.1
1
10
100
1000
thickness H (cm)
number of beds thicker than H
?
contained
non-ponded
turbidites
1
2
3
4
flow
stripping

Table 1

main characterisics	*case study/dataset*			
	Tertiary Piedmont Basin		*Central Apennine foreland basin*	
	Castagnola Fm. (CS)	**Cengio (CTS) and Bric la croce-Castelnuovo (BCTS)**	**Laga Fm. lobes (LG)**	**Cellino Fm. (CL)**
Geodynamic context	Episutural basin on top of Alps-Apennine knot		Foreland basin system of Apennines Wedge-top depozone	Axial foredeep depozone
Age	Late Chattian - Early Burdigalian	Late Oligocene	Late Tortonian-early Late Messinian	Early Piocene
Thickness (m)	>950	350	3000	2500
Studied units Total thickness in brackets	Costa Grande and Arenaceo Members (850 m); Units 1 to 3 (CS-1 to 3 in this work) of Marini et al. 2016	all sandstone bodies of CTS and BCTS (250 m)	Poggio Umbricchio (LG-1) and Crongaleto (LG-2) complexes (Laga 1) and Bilaciere (LG-3) complex (lower Laga 2) (500 m)	lower (CL-1) and upper (CL-2) E Member (750 m)
Geometry of local depocentre	bowl-shaped enclosed (CS-1-2) evolving into larger open-end basin (CS-3)	elongated, enclosed (?) trough	enclosed mini-basin to laterally confined trough	elongated, enclosed
Approximate average size of local depocentre (Lenght x Width)	10 x 7 km (?, CS-1); size of depocentre uncknown for CS-2-3 but certainly larger than that of CS-1	> 6 x 4 km (CTS) to > 12 x 6 km (BCTS)	15 x 10 km (LG-1) to > 25 x 20 km (LG-2-3)	40 x 20 km (?, CL-1) to 40 x 40 km (?, CL-2)
Dominant architectural elements	confined sheets (CS-1-2) to unconfiend locally amalgamated obes (CS-3)	confined sheets (lower section, lowernmost CTS) passing into amalgmated lobes (upper CTS and BCTS)	confined sheets (LG-1-2) to unconfined lobes (LG-3)	confined sheets
Sandbody geometries	sheet-like (CS-1-2) to lobate (CS-3)	sheet-like (lower CTS) to lobate (BCTS)	sheet-like (LG-1-2) to lobate (LG-3)	dominantly sheet-like
Sandbody stacking pattern	Flat and aggradational (CS-1-2) to compensational (CS-3)	Flat and aggradational (lower CTS) to compensational (upper CTS and BCTS)	Flat and aggradational (LG-1-2) to compensational (LG-3)	Flat and aggradational
Previous work	Southern et al., 2015; Marini et al. 2016	Bersezio et al. 2005, 2009; Felletti and Bersezio 2010	Milli et al. 2007; Marini et al. 2015	Carruba et al. 2004, 2006, 2007; Felletti et al. 2009

Table 2

case study	strat. subset	depositional context	bed type subset with no. of sample data		best fit	log-normal										power-law										exponential									k
						parmeters		test statistics								parmeters		test statistics								param.	test statistics								no. bins used in Chi-Sq
								K-S			A-D		Chi-Sq					K-S			A-D		Chi-Sq				K-S			A-D		Chi-Sq			
						σ	μ	p	stat.		stat.		p	stat.		β	x_{min}	p	stat.		stat.		p	stat.		λ	p	stat.		stat.		p	stat.		
Castangola Formation	CS-1	ponded	all beds	378	log-normal	1.51	1.62	0	0.13	x	9.17	x	0	52.73	x	-	-	0	0.25	x	29.99	x	0	68.56	x	-	0	0.43	x	153.54	x	0	460.25	x	10
			Tc/Td base	325	exponential	-	-	0	0.16	x	8.62	x	0	92.94	x	-	-	0	0.30	x	37.80	x	0	33.62	x	0.19	0	0.16	x	9.94	x	0	52.11	x	9
			Ta/Tb base	53	power-law	-	-	0.05	0.18	x	2.17	x	0.38	4.21	√	1.97	30	0.49	0.11	√	3.89	x	0.74	2.72	√	-	0.01	0.22	x	3.79	x	0.03	9.19	x	7
	CS-2	partially ponded	all beds	86	log-normal	1.84	1.96	0.01	0.17	x	3.36	x	0.00	17.66	x	-	-	0.00	0.30	x	14.35	x	0	35.55	x	-	0	0.42	x	35.87	x	0	93.32	x	7
			Tc/Td base	58	exponential	-	-	0.0	0.27	x	4.23	x	0.02	10.09	x		-	0.00	0.46	x	-3.87	√	0	42.16	x	0.27	0	0.23	x	4.53	x	0.09	6.50	√	7
			Ta/Tb base	28	power-law	-	-	0.53	0.15	√	0.51	x	0.28	2.55	√	1.19	20	0.64	0.13	√	3.88	x	0.96	0.31	√	-	0.28	0.18	√	0.99	√	0.82	0.66	√	6
	CS-3	unconfined	all beds	175	log-normal	1.44	3.22	0.04	0.11	x	2.81	x	0.05	13.87	x	-	-	0	0.29	x	39.84	x	0	64.65	x	-	0	0.14	x	4.13	x	0	24.08	x	8
			Tc/Td base	80	exponential	-	-	0.03	0.16	x	2.82	x	0.00	21.62	x	-	-	0	0.30	x	23.76	x	0	28.06	x	0.10	0.04	0.15	x	2.32	x	0	21.57	x	7
			Ta/Tb base	95	log-normal	0.64	4.31	0.40	0.09	√	0.85	√	0.45	5.79	√	-	-	0	0.45	x	28.16	x	0	81.48	x	-	0	0.26	x	8.66	x	0	36.95	x	8
Cengio and Bric la croce-Castelnuovo	CTS	partially ponded to confined	all beds	202	log-normal	1.78	2.23	0.05	0.09	x	2.52	x	0.01	17.50	x	-	-	0.00	0.34	x	43.94	x	0.0	206.62	x	-	0	0.18	x	15.75	x	0	37.68	x	9
			Tc/Td base	119	log-normal	1.67	1.30	0.19	0.10	√	9.22	x	0.03	14.09	x	-	-	-	-	-	-	-	-	-	-	-	0	0.19	x	21.31	x	0	22.98	x	8
			Ta/Tb base	83	log-normal	0.90	3.54	0.89	0.06	√	0.35	√	0.83	2.86	√	-	-	0.00	0.41	x	19.87	x	0.0	73.02	x	-	0.04	0.15	x	1.59	√	0.50	4.34	√	7
	BCTS	confined	all beds	341	log-normal	1.26	2.54	0.13	0.06	√	1.39	√	0.22	10.69	√	-	-	0.00	0.31	x	57.38	x	0	307.30	x	-	0	0.13	x	8.41	x	0	37.93	x	9
			Tc/Td base	128	log-normal	0.77	1.35	0.09	0.11	x	1.11	√	0.10	10.58	√	-	-	0.00	0.39	x	24.82	x	0	128.38	x	-	0	0.21	x	5.31	x	0	36.41	x	8
			Ta/Tb base	213	log-normal	0.90	3.26	0.63	0.05	√	0.36	√	0.42	7.05	√	-	-	0.00	0.32	x	42.41	x	0	222.67	x	-	0.03	0.10	x	3.68	x	0	25.34	x	9
Laga Formation lobes	LG-1	partially ponded	all beds	122	log-normal	1.63	3.56	0.49	0.07	√	0.68	√	0.22	8.29	√	-	-	0.00	0.27	x	16.70	x	0.00	56.90	x	-	0	0.22	x	14.43	x	0.0	32.74	x	8
			Tc/Td base	66	exponential	-	-	0.24	0.12	√	1.28	√	0.04	11.66	x	-	-	0.00	0.28	x	10.08	x	0.00	24.81	x	0.06	0.46	0.10	√	0.73	√	0.72	3.68	√	7
			Ta/Tb base	55	power-law	-	-	0.19	0.14	√	1.74	√	0.08	8.48	x	1.06	50	0.87	0.08	√	5.52	x	0.30	6.02	√	-	0.02	0.21	x	2.41	x	0.07	7.21	x	7
	LG-2	confined	all beds	63	log-normal	1.39	4.01	0.99	0.05	√	0.25	√	0.98	0.71	√		-	0.00	0.36	x	14.13	x	0.00	47.64	x		0.14	0.14	√	1.88	√	0.41	5.07	√	7
			Tc/Td base	23	log-normal	0.91	2.56	0.20	0.22	√	1.14	√	0.12	4.17	√	-	-	0.01	0.34	x	6.57	x	0.01	6.12	x	-	0.15	0.23	√	1.38	√	0.45	1.61	√	6
			Ta/Tb base	40	log-normal	0.82	4.85	0.83	0.09	√	0.44	√	0.71	2.15	√	-	-	0.17	0.17	√	3.59	x	0.21	5.86	√	-	0.15	0.17	√	1.25	√	0.88	1.16	√	6
	LG-3	unconfined	all beds	91	log-normal	1.21	3.84	0.36	0.10	√	0.96	√	0.25	7.79	√	-	-	0.00	0.23	x	11.22	x	0.00	21.01	x	-	0.04	0.15	x	3.38	x	0.15	9.54	√	8
			Tc/Td base	42	log-normal	0.64	2.78	0.22	0.16	√	1.36	√	0.34	3.35	√	-	-	0.00	0.37	x	8.11	x	0.72	1.33	x	-	0	0.32	x	3.47	x	0.82	0.40	x	6
			Ta/Tb base	49	log-normal	0.78	4.74	0.62	0.10	√	0.76	√	0.63	2.60	√	-	-	0.14	0.16	√	3.64	x	0.41	3.94	√	-	0.03	0.21	x	1.88	√	0.65	2.46	√	7
Cellino Formation	CL-1	ponded turbidites	all beds	307	log-normal	1.58	1.93	0	0.19	x	16.81	x	0	241.61	x	-	-	0.00	0.21	x	45.86	x	0.00	68.24	x	-	0	0.59	x	229.38	x	0	703.2	x	9
			Tc/Td base	265	log-normal	0.81	1.4	0	0.13	x	2.80	x	0	64.59	x	-	-	0.00	0.29	x	58.29	x	0.00	132.89	x	-	0	0.19	x	10.01	x	0	93.70	x	9
			bouma seq.	24	log-normal	0.55	4.66	0.38	0.18	√	1.14	√	0.10	4.68	√	-	-	0.03	0.29	x	4.65	x	0.04	4.42	x	-	0.06	0.27	x	3.40	x	0.27	2.60	√	6
			'ponded' megabeds	18	power-law	-	-	0.72	0.15	x	0.58	x	0.63	0.91	√	2.54	270	0.70	0.15	√	2.31	x	0.64	0.88	√		0.01	0.37	x	2.34	x	0.22	3.07	√	5
	CL-2	partially ponded	all beds	598	log-normal	1.17	1.12	0	0.22	x	41.32	x	0	250.31	x	-	-	0	0.26	x	147.53	x	0	99.83	x	-	0	0.63	x	514.52	x	0	1710.7	x	10
			Tc/Td base	577	log-normal	0.73	0.95	0	0.16	x	17.57	x	0	108.02	x	-	-	0	0.31	x	155.92	x	0	138.45	x	-	0	0.24	x	39.65	x	0	175.17	x	10
			bouma seq.	8	log-normal	0.26	4.78	0.79	0.21	√	0.45	√	-	-	-	-	-	0.56	0.26	√	2.01	x	-	-	-	-	0.04	0.47	x	2.08	x	-	-	-	-
			'ponded' megabeds	13	log-normal	0.24	6.6	0.84	0.16	√	0.35	√	0.49	0.48	√	-	-	0.06	0.35	x	3.48	x	0.08	3.06	x	-	0.01	0.44	x	3.61	x	-	-	-	-

Table 3

case study/dataset		*type of confinement*	*subset*	*max*	*min*	*mean* (cm)	*interquartile range*	*coef of variation*
Castangola Fm. (CS)		ponded	CS-1	1040	30	140	95	1.41
		partially ponded	CS-2	670	20	105	109	1.22
		unconfined	CS-3	320	5	89	70	0.57
Cengio (CTS) - Bric la croce-Castelnuovo (BCTS)		partially ponded to confined	CTS	432	2	52	43	1.12
		confined	BCTS	410	2	39	32.5	1.08
Laga Formation lobes (LG)		partially ponded	LG-1	892	50	217	199	1.02
		confined	LG-2	740	35	182	152.5	0.95
		unconfined	LG-3	595	35	156	140	0.87
Cellino Formation (CL)	beds starting with a basal Ta/Tb	ponded	CL-1	1270	35	321	302	0.98
		partially ponded	CL-2	1090	79	517	675	0.67
	'ponded' megabeds	ponded	CL-1	1270	270	588	550	0.55
		partially ponded	CL-2	1090	440	759	222	0.23